Divergent Component of Motion Planning and Adaptive Repetitive Control for Wearable Walking Exoskeletons

Pengbo Huang, *Graduate Student Member, IEEE*, Zhijun Li, *Fellow, IEEE*, MengChu Zhou, *Fellow, IEEE*, and Zhen Kan, *Senior Member, IEEE*

***Abstract*—Wearable walking exoskeletons show great potentials in helping patients with neuro musculoskeletal stroke. Key to the successful applications is the design of effective walking trajectories that enable smooth walking for exoskeletons. This work proposes a walking planning method based on the divergent component of motion to obtain a stable joint angle trajectory. Since periodic and nonperiodic disturbances are ubiquitous in the repeating walking motion of an exoskeleton system, a major challenge in the walking control of wearable exoskeleton is the joint angle drift problem, that is, the joint angle motion trajectories are not necessarily periodic due to the presence of disturbance. To address this challenge, this work develops an adaptive repetitive control strategy to guarantee that the motion trajectories of joint angle are repetitive. In particular, by treating the disturbance as system uncertainties, an adaptive controller is designed to compensate for the uncertainties based on an integral-type Lyapunov function. A fully saturated learning approach is then developed to achieve asymptotic tracking of repetitive walking trajectories. Extensive experiments are carried out to demonstrate the effectiveness of the tracking performance.**

***Index Terms*—Adaptive repetitive control, divergent component of motion (DCM), integral-type Lyapunov function, walking exoskeleton.**

Manuscript received 26 May 2022; revised 27 August 2022 and 30 October 2022; accepted 13 November 2022. Date of publication 1 December 2022; date of current version 18 March 2024. This work was supported in part by the National Natural Science Foundation of China under Grant U1913601; in part by the National Key Research and Development Program of China under Grant 2021YFF0501600; in part by the Major Science and Technology Projects of Anhui Province under Grant 202103a05020004; in part by the National Natural Science Foundation of China under Grant U22A2060; and in part by the Ministry of Science and Higher Education of the Russian Federation as part of World-class Research Center Program: Advanced Digital Technologies under Contract 075-15-2020-903. This article was recommended by Associate Editor N. Zhang. *(Corresponding author: Zhijun Li.)*

This work involved human subjects or animals in its research. Approval of all ethical and experimental procedures and protocols was granted by the Ethics Committee of Yueyang Integrated Traditional Chinese and Western Medicine Hospital Affiliated with Shanghai University of Traditional Chinese Medicine under Application No. 2019-014.

Pengbo Huang, Zhijun Li, and Zhen Kan are with the Department of Automation, University of Science and Technology of China, Hefei 230026, China (e-mail: hpb25200@mail.ustc.edu.cn; auzjli@ustc.edu.cn).

MengChu Zhou is with the Department of Electrical and Computer Engineering, New Jersey Institute of Technology, Newark, NJ 07102 USA, and also with the Department of Cyber–Physical Systems, St. Petersburg State Marine Technical University, 198262 St. Petersburg, Russia (e-mail: zhou@njit.edu).

Color versions of one or more figures in this article are available at https://doi.org/10.1109/TCYB.2022.3222564.

Digital Object Identifier 10.1109/TCYB.2022.3222564

I. Introduction

RECENT advances of wearable walking exoskeletons significantly enhance the mobility of patients with neuro musculoskeletal stroke. Such exoskeletons are being gradually deployed into military and rehabilitation fields [1]. The assisted exoskeleton can restore patient's functions after neuro musculoskeletal stroke or enhance the strength of the elderly with dyskinesia when performing a variety of tasks [2], [3], [4], [5], [6]. However, due to the repetitive trajectories of joint angle and the influence of periodic and nonperiodic disturbance, the desired trajectories of exoskeletons cannot be well tracked. Thus, it is paramount to investigate adaptive repetitive control strategies to improve the tracking performance of repetitive motions.

The control system of a walking exoskeleton in general consists of a walking planner and a controller. The walking planner generates a desired trajectory to enable smooth walking while the controller enables trajectory tracking via feedback control. Recent advances in bipedal robots locomotion are mainly based on the divergent component of motion (DCM). DCM is a divergent part of linear inverted pendulum model (LIPM) dynamics and has been employed in trajectory generation for humanoid robots [7]. Shafiee-Ashtiani et al. [8] employed a DCM modulation to develop a unified and robust trajectory generation method. It allows a humanoid robot to walk on uneven terrains. Hopkins et al. [9] used it to generate a dynamic locomotion framework on uneven terrains for a humanoid robot. The trajectory of the height of a generic center of mass (COM) is obtained by considering the natural frequency of DCM as a variable. Englsberger et al. [10] extended the DCM dynamics to three dimensions. They proposed a 3-D walking planning and tracking controller for stable bipedal walking motion. Jeong et al. [11] proposed a DCM adjustment strategy for a biped ankle, hip, and stepping. Motivated by the above research and the similarity between a walking exoskeleton and a bipedal robot, a walking planning method is developed to generate a COM trajectory by using the stable dynamics between DCM and COM. It is worth mentioning that we can obtain joint angle trajectories from COM and ankle trajectories by utilizing inverse kinematics.

Various control strategies have been developed to achieve high tracking performance for wearable walking exoskeletons [12], [13], [14]. Sun et al. [1] proposed a reduced adaptive

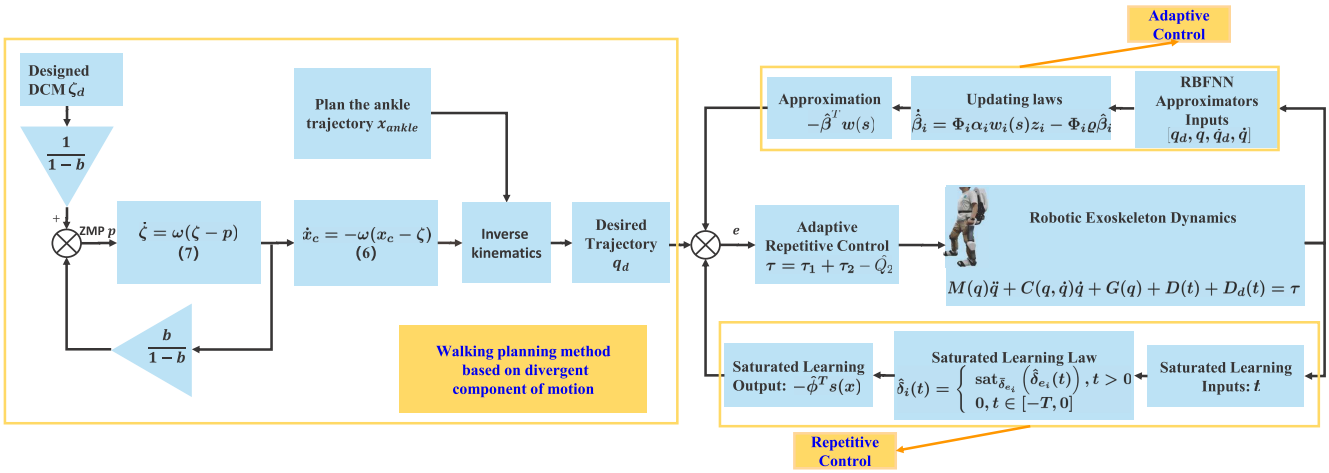

Fig. 1. Proposed control strategy.

fuzzy decoupling control strategy for a lower limb exoskeleton to achieve desired tracking performance. A reduced adaptive fuzzy system and a compensation strategy to effectively reduce chattering phenomena. Zou et al. [4] used a slope gradient estimator and dynamic movement primitives to generate an adaptive gait and then used a proportion integration differentiation controller to achieve the joint position tracking. Martínez et al. [15] proposed a flow controller to provide an effective leg movement guidance for a walking exoskeleton. Li et al. [16] used virtual tunnels and fuzzy strategy to synthesize a human–robot cooperative controller for a walking exoskeleton. The leg motion can be constrained within a specified tunnel around an expected path. In addition, other representative approaches include human-in-the-loop control [17] and optimal control [18], [19], [20], [21]. However, the conventional control strategies mentioned above ignore the periodic repeating leg motion of walking exoskeletons, which plays an important role in assisting the wearer. Hence, it is important and meaningful to develop a repetitive controller for a walking exoskeleton to achieve high tracking performance.

Repetitive control attracts growing attention in robotics [22], due to its capability in handling repetitive tasks in a finite-time interval for a variety of robotic systems, for example, robotic manipulators [23], [24] and permanent magnet synchronous motor servo systems [25]. Existing studies have investigated some repetitive control issues. Verrelli et al. [26] proposed a repetitive control strategy to achieve asymptotic joint position tracking for a robotic manipulator. Li et al. [27] designed a repetitive learning controller for robotic leg prostheses to reduce prosthetic tracking errors. A neural–dynamics optimization strategy is developed to obtain a repetitive joint angle motion trajectory for robotic leg prostheses, which is then tracked using repetitive learning control. Meng et al. [28] used repetitive learning control to generate a novel active disturbance rejection strategy for an inverter system. By utilizing the disturbance and closed-loop data, repetitive control can deal with periodic tracking errors. Motivated by such research, this work integrates repetitive control into a walking exoskeleton to enable trajectory tracking.

Fig. 1 summarizes the proposed control strategy. An integral Lyapunov function is exploited to facilitate the design of an adaptive repetitive controller for walking exoskeletons. When considering nonperiodic and periodic disturbance [29], existing studies are mainly based on prior knowledge or a known robot model. However, a precise model of walking exoskeletons or prior knowledge is generally unavailable in practice. Therefore, we adopt a learning-based solution to approximate the unknown dynamics of a given exoskeleton. To deal with repetitive motion characteristics and periodic unknown disturbance, a fully saturated learning method is developed to improve the tracking performance in the presence of uncertain dynamical models. Rigorous analysis shows that uniformly ultimately bounded convergence is guaranteed for trajectory tracking. Experimental results demonstrate the effectiveness of the proposed controller.

This work aims to make the below contributions:

1) Taking into account DCM, COM, and zero moment point (ZMP), we develop a motion planning method that can generate effective and executable reference trajectories for walking exoskeletons.
2) We develop an adaptive repetitive learning controller to deal with model uncertainties, periodic disturbances, and periodicity of the walking trajectory. Based on an integral Lyapunov function, our rigorous analysis shows that tracking error is uniformly ultimately bounded.
3) In the proposed adaptive repetitive learning control strategy, we exploit saturation learning to ensure the boundedness of the desired control input.

II. Dynamic Walking Design Based on DCM

In this section, we briefly review the DCM dynamics that are the fundamentals of our walking planning approach [30]. We explain how they can be used to represent the overall dynamics of a walking exoskeleton in a state-space form. Moreover, we illustrate the procedure of desired trajectory planning.

A. Divergent Component of Motion

The dynamics of LIPM can be represented as [31]

$$\frac{d}{dt}\mathbf{x_c} = \boldsymbol{A}\mathbf{x_c}(t) + \boldsymbol{B}p(t) \tag{1}$$

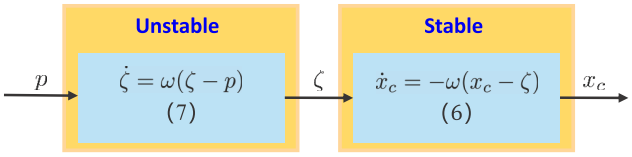

Fig. 2. Coupled dynamics between COM and DCM [32].

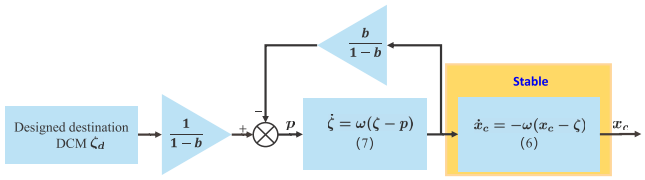

Fig. 3. Strategy for generating the centroid trajectory x_c.

where

$$\mathbf{x_c} = \begin{bmatrix} x_c \\ \dot{x}_c \end{bmatrix}, \boldsymbol{A} = \begin{bmatrix} 0 & 1 \\ \omega^2 & 0 \end{bmatrix}, \boldsymbol{B} = \begin{bmatrix} 0 \\ -\omega^2 \end{bmatrix}, \omega = \sqrt{\frac{g}{h}}.$$

x_c represents the position of COM, p represents the ZMP, g is the gravitational acceleration, and h represents the height of COM. When considering zero input response (i.e., $p = 0$) of (1), the eigenvectors of $\boldsymbol{A}$ are

$$\boldsymbol{v}^- = \begin{bmatrix} 1 \\ -\omega \end{bmatrix} \text{and} \quad \boldsymbol{v}^+ = \begin{bmatrix} 1 \\ \omega \end{bmatrix}$$

which correspond to the eigenvalues ω and $-\omega$, respectively. Given $\boldsymbol{V} = [\boldsymbol{v}^-, \boldsymbol{v}^+]$, we define

$$\begin{bmatrix} \eta \\ \zeta \end{bmatrix} = \boldsymbol{V}^{-1} \begin{bmatrix} x_c \\ \dot{x}_c \end{bmatrix}. \tag{2}$$

Substituting (2) into (1), we can rewrite the dynamics as

$$\frac{d}{dt} \begin{bmatrix} \eta \\ \zeta \end{bmatrix} = \boldsymbol{V}^{-1} \boldsymbol{A} \boldsymbol{V} \begin{bmatrix} \eta \\ \zeta \end{bmatrix} = \begin{bmatrix} -\omega & 0 \\ 0 & \omega \end{bmatrix} \begin{bmatrix} \eta \\ \zeta \end{bmatrix}. \tag{3}$$

Solving (3) yields

$$\begin{aligned} \eta(t) &= C_1 e^{-\omega t} \\ \zeta(t) &= C_2 e^{\omega t} \end{aligned} \tag{4}$$

where C_1 and C_2 are nonzero constants. Equation (4) shows that η converges but ζ diverges as time proceeds. Hence, we only need to consider the divergent item ζ when designing the COM of LIPM.

According to (2) and (3), we obtain the DCM dynamics

$$\zeta = x_c + \frac{\dot{x}_c}{\omega}. \tag{5}$$

Solving (5) for x_c, we have

$$\dot{x}_c = -\omega(x_c - \zeta). \tag{6}$$

By differentiating (5) and using (6) and (1), we have

$$\dot{\zeta} = \dot{x}_c + \frac{\ddot{x}_c}{\omega} = \omega(\zeta - p). \tag{7}$$

B. DCM Control

In order to obtain the trajectory of the joint angle, we need to find the trajectory of COM. Motivated by [32], by considering (6) and Fig. 2, we use DCM dynamics (7) to plan a COM trajectory. Considering a constant ZMP p, we can obtain the solution of (7) as follows:

$$\zeta(t) = e^{\omega t}\zeta_0 + \left(1 - e^{\omega t}\right)p. \tag{8}$$

Considering the dynamic update process of ζ, we replace initial ζ_0 with the current DCM ζ and rewrite (8) as

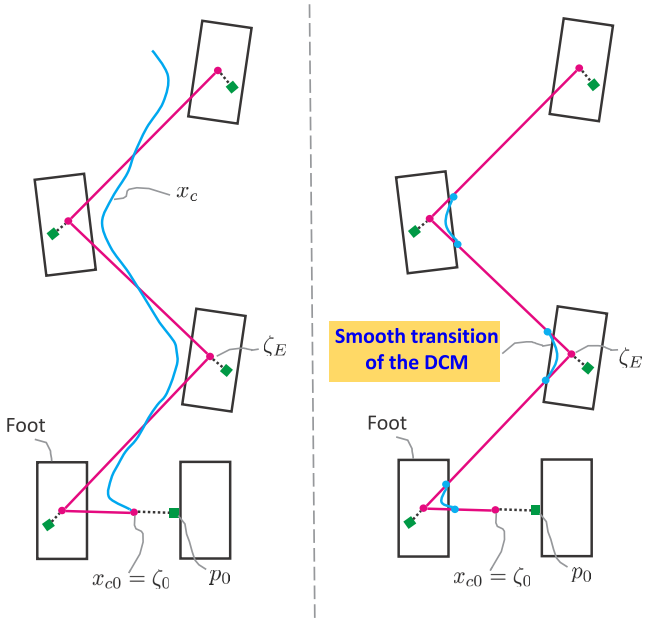

Fig. 4. Shifting DCM from one foot to another foot (left) and smoothing the DCM reference trajectory (right).

$$p = \frac{\zeta_d - e^{\omega d_T}\zeta}{1 - e^{\omega d_T}} = \frac{1}{1-b}\zeta_d - \frac{b}{1-b}\zeta \tag{9}$$

where d_T represents the time span to reach the desired DCM position ζ_d and $b = e^{\omega d_T}$ and ζ_d represents $\zeta_d(t)$. This control law is summarized in Fig. 3, and [32] proves its stability. In general, we can hold the constant ZMP in the middle of the foot in order to obtain a stable walking gait. Constant ZMP has advantages in comparison with nonconstant ZMP. Nonconstant ZMP may increase the risk of the robot's falling, because ZMP may be at the edge of the support polygon. The support polygon represents the support area to keep a robot walking stably [33]. Therefore, we keep ZMP as a constant to ensure that ZMP is always within the feasible support polygon region.

Fig. 4 shows a schematic of the robot's walking steps. DCM is shifted from one footprint to the next during each step. ζ_E represents the desired DCM position at the end of a step. Considering the relation between COM and DCM as shown in (5), exoskeleton can shift its COM from the initial COM position x_{c0} to the final one. ζ_E and the desired step time are used to obtain a reference DCM ζ_R to be introduced next.

C. Reference Trajectory Generation of DCM

In order to generate the reference trajectory of DCM, we define the span of time d_T as a constant value. ζ_E is the target point of DCM for each step as shown in Fig. 4. According to ζ_E and (9), we obtain the desired constant ZMP. Then, we

can calculate a reference ζ_R for each time step via (8) and the desired ZMP. According to (8), DCM is shifted within d_T to the position in which the reference ζ_R would be at $t+d_T$ [32]. Therefore, we set desired DCM $\zeta_d(t) = \zeta_R(t+d_T)$ in (9). We set $\zeta_d = [\zeta_d^x, \zeta_d^y]$, where ζ_d^x represents desired DCM in the x-axis direction and ζ_d^y represents desired DCM in the y-axis direction.

D. Smoothing DCM Reference Trajectory

Fig. 4 (left) shows a schematic of the original DCM reference trajectory, which leads to a zigzag trajectory [red lines in Fig. 4 (left)]. It represents the discontinuity of the first derivative of DCM, and further, this leads to the discontinuity of the first derivative of the generated COM trajectory, which may cause damage to the wearer of the walking exoskeleton when the wearer switches between left and right feet to walk. Fig. 4 (right) shows the outline for the generation of DCM trajectory with smoothing transitions. The DCM trajectory generation builds on the idea proposed in [10], which leads to a smooth DCM reference trajectory to guarantee continuity of the first derivative of the DCM. The basic idea of the approach we chose is using a sixth degree polynomial to round the DCM. A polynomial parameter matrix can be constructed as

$$\boldsymbol{P_t} = \begin{bmatrix} 1 & 1 & 1 & 0 & 0 & 0 & 0 \\ 0 & T_t/2 & T_t & 1 & 1 & 0 & 0 \\ 0 & (T_t/2)^2 & (T_t)^2 & 0 & 2T_t & 2 & 2 \\ 0 & (T_t/2)^3 & (T_t)^3 & 0 & 3(T_t)^2 & 0 & 6T_t \\ 0 & (T_t/2)^4 & (T_t)^4 & 0 & 4(T_t)^3 & 0 & 12(T_t)^2 \\ 0 & (T_t/2)^5 & (T_t)^5 & 0 & 5(T_t)^4 & 0 & 20(T_t)^3 \\ 0 & (T_t/2)^6 & (T_t)^6 & 0 & 6(T_t)^5 & 0 & 30(T_t)^4 \end{bmatrix} \tag{10}$$

where T_t represents the total length of ζ_d^x for smooth transition as shown in Fig. 4. With P_t, for any $\zeta_d^x \in [0, T_t]$, the ζ_d^y DCM position can be computed as

$$\zeta_d^y = \boldsymbol{P_b} \boldsymbol{P_t}^{-1} \boldsymbol{P_\zeta} \tag{11}$$

where $\boldsymbol{P_b} = [\zeta_A\ \zeta_B\ \zeta_C\ \dot{\zeta}_A\ \dot{\zeta}_C\ \ddot{\zeta}_A\ \ddot{\zeta}_C]$, $\boldsymbol{P_\zeta} = [1\ \zeta_d^x\ \zeta_d^{x2}\ \zeta_d^{x3}\ \zeta_d^{x4}\ \zeta_d^{x5}\ \zeta_d^{x6}]^T$. $\zeta_A, \zeta_B, \zeta_C, \dot{\zeta}_A, \dot{\zeta}_C, \ddot{\zeta}_A$ and $\ddot{\zeta}_C$ are boundary conditions. $\zeta_A, \dot{\zeta}_A$, and $\ddot{\zeta}_A$ denote the initial ζ_d^y position, velocity, and acceleration, respectively. $\zeta_C, \dot{\zeta}_C$, and $\ddot{\zeta}_C$ represent the final DCM position, velocity, and acceleration, respectively. ζ_B represents the ζ_d^y position at the middle moment of $\boldsymbol{P_t}$.

So far, we can obtain a continuous differentiable ζ_d trajectory and COM one, as shown in Figs. 5 and 6. We need to plan the trajectory of the ankle joint of the exoskeleton, and then we can get the trajectory of the joint angle of the walking exoskeleton by inverse kinematics [34], [35].

E. Walking Trajectory Generation

Cubic spline interpolation is a common method in trajectory planning [36]. Motivated by [36], in this work, we use specific time points as the foot constraint conditions and then we use cubic spline interpolation to interpolate the ankle trajectory $p_f = [x_f, z_f]$, where x_f represents the trajectory of the ankle on the sagittal plane and z_f represents the trajectory of the ankle on the vertical plane. Noting that the trajectory of the ankle is periodic, so we only consider $t \in [0, T_S]$. The foot constraint conditions are shown as

$$x_f(t) = \begin{cases} 0, & t = 0 \\ \frac{L_s}{2}, & t = t_X \\ L_s, & t = T_S \end{cases} \tag{12}$$

and

$$z_f(t) = \begin{cases} 0, & t = 0 \\ h_f, & t = t_Z \\ 0, & t = T_S \end{cases} \tag{13}$$

where L_s denotes the step length, t_X denotes the time when the ankle reaches $(L_s/2)$, and t_Z denotes the time when the ankle reaches the highest ankle lift height h_f. Finally, we use the generated position x_c of the COM and the foot trajectory, which are translated to the commanded joint angles using the inverse kinematics of the robot.

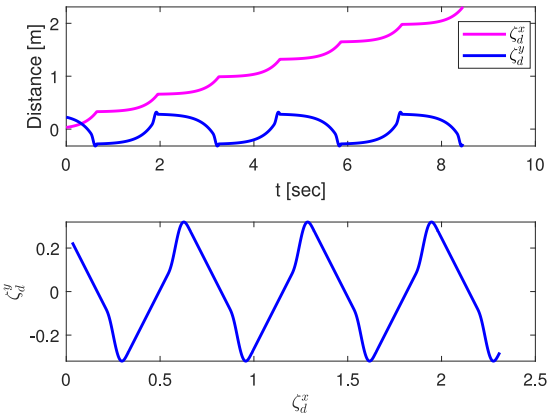

Fig. 5. Continuous differentiable desired ζ_d trajectory.

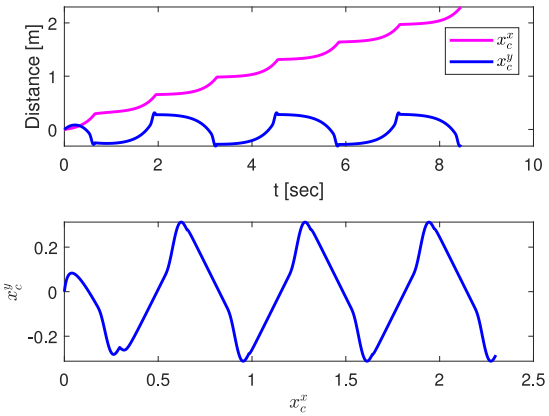

Fig. 6. Continuous differentiable x_c trajectory.

III. Adaptive Repetitive Walking Control Design

A. Dynamics of Wearable Walking Exoskeleton

Following [37], the dynamics of a lower-limb exoskeleton can be written as

$$\boldsymbol{M(q)}\ddot{\boldsymbol{q}} + \boldsymbol{C}(\boldsymbol{q}, \dot{\boldsymbol{q}})\dot{\boldsymbol{q}} + \boldsymbol{G(q)} + \boldsymbol{D(t)} + \boldsymbol{D_d(t)} = \boldsymbol{\tau} \tag{14}$$

where $\boldsymbol{M(q)} \in \mathbb{R}^{n\times n}$ represents an inertia term, $\boldsymbol{C(q, \dot{q})} \in \mathbb{R}^{n\times n}$ is a centripetal and Coriolis term, $\boldsymbol{G(q)} \in \mathbb{R}^n$ denotes

a gravity vector, $\boldsymbol{D(t)} \in \mathbb{R}^n$ represents frictional force and disturbance, $\boldsymbol{D_d(t)} \in \mathbb{R}^n$ represents nonperiodic disturbance, $\boldsymbol{\tau} \in \mathbb{R}^n$ denotes a control torque vector, and $\boldsymbol{q} \in \mathbb{R}^n$ is a joint angle vector.

We define $\boldsymbol{x_1} = \boldsymbol{q}$, $\boldsymbol{x_2} = \dot{\boldsymbol{q}}$, $\boldsymbol{x} = [\boldsymbol{x_1}^T, \boldsymbol{x_2}^T]^T$, and denote the desired walking trajectory for the exoskeleton as $\boldsymbol{q_d} \in \mathbb{R}^n$. By substituting $\boldsymbol{x_1}$, $\boldsymbol{x_2}$, and $\dot{\boldsymbol{x}}_1 = \boldsymbol{x_2}$ into (14), we can rewrite it in a state-space form as

$$\begin{cases} \dot{\boldsymbol{x}}_1 = \boldsymbol{x_2} \\ \dot{\boldsymbol{x}}_2 = \\ \boldsymbol{M}^{-1}(\boldsymbol{q})\big[-\boldsymbol{C}\big(\boldsymbol{q}, \dot{\boldsymbol{q}}\big)\boldsymbol{x_2} - \boldsymbol{G}(\boldsymbol{q}) - \boldsymbol{D}(\boldsymbol{t}) - \boldsymbol{D_d}(\boldsymbol{t}) + \boldsymbol{\tau}\big]. \end{cases} \tag{15}$$

Assumption 1: The desired trajectory $\boldsymbol{q_d}$ is periodic with known period T and $\boldsymbol{D(t)}$ is also periodic with the same period [27], that is, $\boldsymbol{q_d(t)} = \boldsymbol{q_d(t-T)}$ and $\boldsymbol{D(t)} = \boldsymbol{D(t-T)}$.

Remark 1: Assumption 1 implies that the desired trajectory $\boldsymbol{q_d}$ and its derivative $\dot{q}_d$ as well as the disturbance $\boldsymbol{D(t)}$ are periodic.

Let $\boldsymbol{\Delta_M} \in \mathbb{R}^{n\times n}$ be the model uncertainty. $\boldsymbol{M(q)}$ can be rewritten as

$$\boldsymbol{M(q)} = \boldsymbol{M_d(q)} + \boldsymbol{\Delta_M(q)} \tag{16}$$

where $\boldsymbol{M_d(q)} = \text{diag}[M_{d11}(q), \ldots, M_{dnn}(q)]$ represents the known nominal model. For simplicity, let us use $\boldsymbol{\Delta_M}$ to represent $\boldsymbol{\Delta_M(q)}$. According to (15), (16) can be rewritten as

$$\boldsymbol{M_d(q)}\dot{\boldsymbol{x}}_2 = \boldsymbol{P(x)} + \boldsymbol{\tau} + \boldsymbol{Q} \tag{17}$$

where $\boldsymbol{P(x)} = (I - \boldsymbol{\Delta_M M^{-1}(q)})(-\boldsymbol{C(q,\dot{q})x_2} - \boldsymbol{G(q)}) \in \mathbb{R}^n$ and $\boldsymbol{Q} = \boldsymbol{Q_1} + \boldsymbol{Q_2}$. We define $\boldsymbol{Q_1} = -(I - \boldsymbol{\Delta_M M^{-1}(q)})\boldsymbol{D(t)}$ and $\boldsymbol{Q_2} = -\boldsymbol{\Delta_M M^{-1}(q)\tau} - (I - \boldsymbol{\Delta_M M^{-1}(q)})\boldsymbol{D_d(t)}$. According to [37], we obtain the following result.

Lemma 1: If $\mathcal{F}(t)$ is differentiable continuous, $\forall t \in [t_0, t_1]$, it satisfies $\delta_1 \le ||\mathcal{F}(t)|| \le \delta_2$, and δ_1 and δ_2 are positive constants, then its derivative $\dot{\mathcal{F}}(t)$ is bounded.

Proof: According to the Lagrange mean-value theorem, $\forall\, t$, we obtain $\mathcal{F}(t) - \mathcal{F}(0) = \dot{\mathcal{F}}(\xi)(t-0)$ where $\xi \in (0, t)$. Due to $\delta_1 \le ||\mathcal{F}(t)|| \le \delta_2$, $\delta_1 - \delta_2 \le \mathcal{F}(t) - \mathcal{F}(0) \le \delta_2 - \delta_1$ is bounded, it follows that $\dot{\mathcal{F}}(t)$ is bounded. ■

Assumption 2: According to Lemma 1, if we assume that $\boldsymbol{Q_2}$ is bounded, then $\boldsymbol{Q_2}$ and $\dot{\boldsymbol{Q}}_2$ are all bounded, where $\dot{\boldsymbol{Q}}_2$ represents the first derivative of $\boldsymbol{Q_2}$, that is, $\forall\, t \in \mathbb{R}^+$, $||\boldsymbol{Q_2}||$ and $||\dot{\boldsymbol{Q}}_2||$ are all less than an unknown positive constant.

Remark 2: According to [38], input saturation is universal for a physical actuator and the input torque $\boldsymbol{\tau}$ is saturated in practical nonlinear system. $\boldsymbol{M(q)}$ represents the bounded inertia matrix [39], and $\boldsymbol{\Delta_M}$ is a part of the inertia matrix, which is also bounded. Therefore, we can conclude that $\boldsymbol{Q_2}$ is bounded. According to Lemma 1, $\dot{\boldsymbol{Q}}_2$ is also bounded.

B. Control Design

The control objective is to find a controller $\boldsymbol{\tau}$ such that the output $\boldsymbol{x_1}$ follows a given reference signal $\boldsymbol{q_d}$. Define the following position error $\boldsymbol{e}$ and filtered error z:

$$\boldsymbol{e} = \boldsymbol{x_1} - \boldsymbol{q_d} \tag{18}$$

$$z = \Lambda \boldsymbol{e} + \dot{\boldsymbol{e}} \tag{19}$$

where Λ is a diagonal positive constant matrix. According to (15) and (19), we have

$$\dot{z} = \boldsymbol{M_d^{-1}(q)}\big[\boldsymbol{P(x)} + \boldsymbol{Q} + \boldsymbol{\tau}\big] + \boldsymbol{\nu} \tag{20}$$

where $\boldsymbol{\nu} = [\nu_1, \ldots, \nu_n]^T$ with

$$\boldsymbol{\nu} = -\ddot{\boldsymbol{q}}_{\boldsymbol{d}} + \Lambda \dot{\boldsymbol{e}}. \tag{21}$$

Let $\boldsymbol{\nu_f} = \dot{\boldsymbol{q}}_{\boldsymbol{d}} - \Lambda \boldsymbol{e}$. Then $\boldsymbol{\nu} = -\dot{\boldsymbol{\nu}}_{\boldsymbol{f}}$. According to (16), $\boldsymbol{M_d}$ can be defined as a known model. Thus we can choose $\boldsymbol{M_d} = \boldsymbol{M_d}(\boldsymbol{x_1}, \theta z + \boldsymbol{\nu_f})$. For the convenience of a controller's design, the following scalar function is adopted:

$$\mathcal{V}_f = z^{\boldsymbol{T}}\boldsymbol{B_\theta} z = \sum_{i=1}^{n} z_i^2 \int_0^1 \theta B_{\alpha_{ii}}\big(x_{1i}, \theta z_i + \nu_{f_i}\big)d\theta \tag{22}$$

where $\boldsymbol{B_\theta} = \int_0^1 \theta \boldsymbol{B_\alpha}(\boldsymbol{x_1}, \theta z + \boldsymbol{\nu_f})d\theta$ and $\boldsymbol{B_\alpha}(\boldsymbol{x_1}, \theta z + \boldsymbol{\nu_f}) = \boldsymbol{M_d}(\boldsymbol{x_1}, \theta z + \boldsymbol{\nu_f})\alpha = \text{diag}[B_{\alpha_{11}}, \ldots, B_{\alpha nn}]$. $\alpha = \text{diag}[\alpha_{11}, \ldots, \alpha_{\text{nn}}]$, and θ is a scalar independent of $z, \boldsymbol{x}$, and $\boldsymbol{\nu_f}$.

Taking the time derivative of $\mathcal{V}_f$ in (22), we have

$$\begin{aligned} \dot{\mathcal{V}}_f &= 2z^{\boldsymbol{T}}\boldsymbol{B_\theta}\dot{z} + z^{\boldsymbol{T}}\left(\frac{\partial \boldsymbol{B_\theta}}{\partial z}\dot{z}\right)z \\ &\quad + z^{\boldsymbol{T}}\left(\frac{\partial \boldsymbol{B_\theta}}{\partial \boldsymbol{x_1}}\dot{\boldsymbol{x}}_1\right)z + z^{\boldsymbol{T}}\left(\frac{\partial \boldsymbol{B_\theta}}{\partial \boldsymbol{\nu_f}}\dot{\boldsymbol{\nu}}_{\boldsymbol{f}}\right)z \\ &= 2z^{\boldsymbol{T}}\boldsymbol{B_\theta}\dot{z} + z^{\boldsymbol{T}}\boldsymbol{B_\alpha}\dot{z} - 2z^{\boldsymbol{T}}\boldsymbol{B_\theta}\dot{z} \\ &\quad + \sum_{i=1}^{n} z_i^2 \int_0^1 \theta\left[\frac{\partial B_{\alpha_{ii}}}{\partial x_{1i}}\dot{x}_{1i} + \frac{\partial B_{\alpha_{ii}}}{\partial \nu_{f_i}}\dot{\nu}_{f_i}\right]d\theta \\ &= z^{\boldsymbol{T}}\boldsymbol{B_\alpha}\dot{z} + \sum_{i=1}^{n} z_i^2 \int_0^1 \theta\left[\frac{\partial B_{\alpha_{ii}}}{\partial x_{1i}}\dot{x}_{1i} + \frac{\partial B_{\alpha_{ii}}}{\partial \nu_{f_i}}\dot{\nu}_{f_i}\right]d\theta. \end{aligned} \tag{23}$$

According to [40] and (22), we know $z_i(\partial B_{\alpha_{ii}}/\partial \nu_{f_i}) = (\partial B_{\alpha_{ii}}/\partial\theta)$. Since $\dot{\boldsymbol{\nu}}_{\boldsymbol{f}} = -\boldsymbol{\nu}$, we have

$$\begin{aligned} \sum_{i=1}^{n} z_i^2 \int_0^1 \theta\left[\frac{\partial B_{\alpha_{ii}}}{\partial \nu_{f_i}}\dot{\nu}_{f_i}\right]d\theta &= z^{\boldsymbol{T}}\int_0^1 \theta\left[\frac{\partial \boldsymbol{B_\alpha}}{\partial \boldsymbol{\nu_f}}\dot{\boldsymbol{\nu}}_{\boldsymbol{f}}\right]z d\theta \\ &= -z^{\boldsymbol{T}}\int_0^1 \theta\left[\frac{\partial \boldsymbol{B_\alpha}}{\partial \theta}\boldsymbol{\nu}\right]d\theta \\ &= -z^{\boldsymbol{T}}\boldsymbol{B_\alpha}\boldsymbol{\nu} + z^{\boldsymbol{T}}\int_0^1 \boldsymbol{B_\alpha}\boldsymbol{\nu}d\theta. \end{aligned} \tag{24}$$

We have $\sum_{i=1}^{n} z_i^2 \int_0^1 \theta[(\partial B_{\alpha_{ii}}/\partial x_{1i})\dot{x}_{1i}]d\theta = z^{\boldsymbol{T}}\int_0^1 \theta[(\partial \boldsymbol{B_\alpha}/\partial \boldsymbol{x_1})\dot{\boldsymbol{x}}_1]z d\theta$. Substituting (24) into (23) and using (20), we obtain

$$\begin{aligned} \dot{\mathcal{V}}_f &= z^{\boldsymbol{T}}\alpha\big[\boldsymbol{P(x)} + \boldsymbol{Q_1} + \boldsymbol{Q_2} + \boldsymbol{\tau}\big] \\ &\quad + z^{\boldsymbol{T}}\int_0^1 \boldsymbol{B_\alpha}\boldsymbol{\nu}d\theta + z^{\boldsymbol{T}}\int_0^1 \theta\left[\frac{\partial \boldsymbol{B_\alpha}}{\partial \boldsymbol{x_1}}\dot{\boldsymbol{x}}_1\right]z d\theta. \end{aligned} \tag{25}$$

We define $\boldsymbol{H(x)} = \boldsymbol{P(x)} + \boldsymbol{h(x)}$ and $\boldsymbol{h(x)} = \int_0^1 \boldsymbol{M_d}\boldsymbol{\nu}d\theta + z^{\boldsymbol{T}}\int_0^1 \theta[(\partial \boldsymbol{M_d}/\partial \boldsymbol{x_1})\dot{\boldsymbol{x}}_1]z d\theta$. According to [42], we assume that $\boldsymbol{H(x)}$ and $\boldsymbol{Q_1}$ can be parameterized as

$$\boldsymbol{H(x)} = \boldsymbol{\beta}^{\boldsymbol{T}}\boldsymbol{w(x)} \tag{26}$$

$$\boldsymbol{Q_1} = \boldsymbol{\phi}^{\boldsymbol{T}}\boldsymbol{s(x)} \tag{27}$$

where $\boldsymbol{\beta}^{\boldsymbol{T}} = [\boldsymbol{\beta_1}^{\boldsymbol{T}}, \boldsymbol{\beta_2}^{\boldsymbol{T}}, \ldots, \boldsymbol{\beta_n}^{\boldsymbol{T}}]^T$ denotes the optimal constant weight matrix with $\boldsymbol{\beta_i} \in \mathbb{R}^l$, $\boldsymbol{w(x)} =$

$[w_1(x), w_2(x), \ldots, w_l(x)]^T$ denotes the regressor vector, $\boldsymbol{\phi^T} \in \mathbb{R}^{n\times n}$ is the regressor weight matrix, and $\boldsymbol{s(x)} \in \mathbb{R}^n$ represents a regressor vector. In practical application, we can choose model-free or other parametric methods to deal with $\boldsymbol{H(x)}$ and $\boldsymbol{Q_1}$.

Given the expressions in (26), we have

$$\dot{\mathcal{V}}_f = z^T\alpha\Big[\boldsymbol{\beta^T w(x)} + \boldsymbol{Q} + \boldsymbol{\tau}\Big]. \tag{28}$$

According to the above analysis, one has the following ideal control:

$$\boldsymbol{\tau} = -\alpha^{-1}\kappa z - \boldsymbol{\beta^T w(x)} \tag{29}$$

where κ is a positive definite constant matrix with appropriate dimensions.

Substituting (29) into (28), we obtain

$$\dot{\mathcal{V}}_f = -\boldsymbol{z^T}\kappa z + \boldsymbol{z^T}\alpha\boldsymbol{\phi^T s(x)} + \boldsymbol{z^T}\alpha\boldsymbol{Q_2}. \tag{30}$$

Remark 3: When there exists disturbance, that is, $\phi \neq 0$, the system stability cannot be ensured if the controller in (30) is used. Thus, we have to introduce an additional controller to deal with the unknown time varying uncertainty. In this article, we combine the feedback controller (29) with a repetitive control strategy to compensate for time varying uncertainty. We use an adaptive repetitive control law to estimate ϕ in order to obtain an effective compensation performance. In addition, we use a disturbance observer to deal with $\boldsymbol{Q_2}$.

C. Adaptive Repetitive Control

The saturation function is defined as $\text{sat}_{\bar{\boldsymbol{d}}}(\boldsymbol{d}) = \text{diag}[\,\text{sat}_{\bar{d}_1}(d_1), \ldots, \text{sat}_{\bar{d}_n}(d_n)]^T \in \mathbb{R}^{n\times n}$ with

$$\text{sat}_{\bar{d}_i}(d_i) = \begin{cases} \bar{d}_i^1, & d_i < \bar{d}_i^1 \\ d_i, & \bar{d}_i^1 \le d_i \le \bar{d}_i^2 \\ \bar{d}_i^2, & d_i > \bar{d}_i^2 \end{cases} \tag{31}$$

where $i = 1, 2, \ldots, n$, and d_i is a scalar. We use $*$ to represent a scalar. $\bar{*}^1$ and $\bar{*}^2$ represent the lower and upper bounds of $*$, respectively. We define $\boldsymbol{b} = [b_1, \ldots, b_n] \in \mathbb{R}^{n\times n}$.

Lemma 2 [44]: For d_i and b_i, if we have $\bar{b}_i^1 \le d_i \le \bar{b}_i^2$, $i = 1, 2, \ldots, n$, then

$$\Big[(\gamma+1)d_i - \Big(\gamma b_i + \text{sat}_{\bar{b}_i}(b_i)\Big)\Big]^T \Lambda\Big[b_i - \text{sat}_{\bar{b}_i}(b_i)\Big] \le 0 \tag{32}$$

where $\gamma \ge 0$ is a scalar and $\Lambda > 0$ is also a scalar.

Consider the following repetitive control:

$$\boldsymbol{\tau} = \boldsymbol{\tau_1} + \boldsymbol{\tau_2} \tag{33}$$

where the feedback controller is $\boldsymbol{\tau_1} = -\alpha^{-1}\kappa z - \boldsymbol{\beta^T w(x)}$, and $\boldsymbol{\tau_2}$ is a repetitive controller given as

$$\boldsymbol{\tau_2} = -\hat{\boldsymbol{\phi}}^{\boldsymbol{T}}\boldsymbol{s(x)} \tag{34}$$

with the estimate for $\boldsymbol{\phi}$ that is updated by the partially saturated learning law

$$\hat{\boldsymbol{\phi}}(\boldsymbol{t}) = \begin{cases} \text{sat}_{\bar{\boldsymbol{\phi}}_{\boldsymbol{T}}}\Big(\hat{\boldsymbol{\phi}}_{\boldsymbol{T}}(\boldsymbol{t})\Big) + \boldsymbol{R(t)}, & t > 0 \\ 0, & t \in [-T, 0] \end{cases} \tag{35}$$

where $\boldsymbol{R(t)} = \text{diag}[\Gamma_1\alpha_1 s_1(x) z_1, \ldots, \Gamma_n\alpha_n s_n(x) z_n]$, $\hat{\phi}(t) = \text{diag}[\hat{\phi}_1(t), \ldots, \hat{\phi}_n(t)]$, $\Gamma = \text{diag}[\Gamma_1, \ldots, \Gamma_n]$ is a positive diagonal matrix, $\hat{\boldsymbol{\phi}}_{\boldsymbol{T}}(\boldsymbol{t}) = \hat{\boldsymbol{\phi}}(\boldsymbol{t-T})$, and $\bar{\phi}_T = [\bar{\phi}_{T_1}, \bar{\phi}_{T_2}]$ represents the bounded value. For simplicity, we use $\hat{\phi}_i$ to represent $\hat{\phi}_i(t)$.

Combining (28) and (33), we can obtain

$$\dot{\mathcal{V}}_f = -\boldsymbol{z^T}\kappa z + \boldsymbol{z^T}\alpha\tilde{\boldsymbol{\phi}}^{\boldsymbol{T}}\boldsymbol{s(x)} + \boldsymbol{z^T}\alpha\boldsymbol{Q_2} \tag{36}$$

where $\tilde{\boldsymbol{\phi}} = \boldsymbol{\phi} - \hat{\boldsymbol{\phi}}$.

Define the Lyapunov function candidate

$$\mathcal{V}_1 = \mathcal{V}_f + \mathcal{V}_r \tag{37}$$

with

$$\mathcal{V}_r = (1/2)\sum_{i=1}^{n}\int_{t-T}^{t}\tilde{\phi}_i(\tau)\Gamma_i^{-1}\tilde{\phi}_i(\tau)d\tau. \tag{38}$$

By Lemma 2, for the case $\gamma = 1$, we have

$$\Big[2\phi_i - \hat{\phi}_{T_i} - \text{sat}_{\bar{\phi}_{T_i}}\Big(\hat{\phi}_{T_i}\Big)\Big]\Gamma_i^{-1}\Big[\hat{\phi}_{T_i} - \text{sat}_{\bar{\phi}_{T_i}}\Big(\hat{\phi}_{T_i}\Big)\Big] \le 0. \tag{39}$$

We use $\boldsymbol{\phi_T}$ to represent $\boldsymbol{\phi(t-T)}$, and $\boldsymbol{\phi_T} = \text{diag}[\phi_{T_i}, \ldots, \phi_{T_n}] \in \mathbb{R}^{n\times n}$. We take the derivative of $\mathcal{V}_r$ to obtain

$$\dot{\mathcal{V}}_r = \sum_{i=1}^{n}\frac{1}{2}\Big[\tilde{\phi}_i\Gamma_i^{-1}\tilde{\phi}_i - \Big(\phi_{T_i} - \hat{\phi}_{T_i}\Big)\Gamma_i^{-1}\Big(\phi_{T_i} - \hat{\phi}_{T_i}\Big)\Big]. \tag{40}$$

Using $(\phi_{T_i} - \hat{\phi}_{T_i})\Gamma_i^{-1}(\phi_{T_i} - \hat{\phi}_{T_i})$ and $\boldsymbol{\phi(t-T)} = \boldsymbol{\phi(t)}$, we have

$$\begin{aligned}
&\Big(\phi_{T_i} - \hat{\phi}_{T_i}\Big)\Gamma_i^{-1}\Big(\phi_{T_i} - \hat{\phi}_{T_i}\Big) \\
&= \phi_{T_i}\Gamma_i^{-1}\phi_{T_i} - 2\phi_i\Gamma_i^{-1}\hat{\phi}_{T_i} + \hat{\phi}_{T_i}\Gamma_i^{-1}\hat{\phi}_{T_i} \\
&= \phi_{T_i}\Gamma_i^{-1}\phi_{T_i} - 2\phi_i\Gamma_i^{-1}\hat{\phi}_{T_i} + \hat{\phi}_{T_i}\Gamma_i^{-1}\hat{\phi}_{T_i} \\
&\quad + 2\phi_i\Gamma_i^{-1}\,\text{sat}_{\bar{\phi}_{T_i}}\Big(\hat{\phi}_{T_i}\Big) - 2\phi_{T_i}\Gamma_i^{-1}\,\text{sat}_{\bar{\phi}_{T_i}}\Big(\hat{\phi}_{T_i}\Big) \\
&\quad + \text{sat}_{\bar{\phi}_{T_i}}\Big(\hat{\phi}_{T_i}\Big)\Gamma_i^{-1}\,\text{sat}_{\bar{\phi}_{T_i}}\Big(\hat{\phi}_{T_i}\Big) \\
&\quad - \text{sat}_{\bar{\phi}_{T_i}}\Big(\hat{\phi}_{T_i}\Big)\Gamma_i^{-1}\,\text{sat}_{\bar{\phi}_{T_i}}\Big(\hat{\phi}_{T_i}\Big) \\
&\quad + \text{sat}_{\bar{\phi}_{T_i}}\Big(\hat{\phi}_{T_i}\Big)\Gamma_i^{-1}\hat{\phi}_{T_i} - \hat{\phi}_{T_i}\Gamma_i^{-1}\,\text{sat}_{\bar{\phi}_{T_i}}\Big(\hat{\phi}_{T_i}\Big) \\
&= \Big(\phi_{T_i} - \text{sat}_{\bar{\phi}_{T_i}}\Big(\hat{\phi}_{T_i}\Big)\Big)\Gamma_i^{-1}\Big(\phi_{T_i} - \text{sat}_{\bar{\phi}_{T_i}}\Big(\hat{\phi}_{T_i}\Big)\Big) \\
&\quad - \Big(2\phi_i - \text{sat}_{\bar{\phi}_{T_i}}\Big(\hat{\phi}_{T_i}\Big) - \hat{\phi}_{T_i}\Big)\Gamma_i^{-1}\Big(\hat{\phi}_{T_i} - \text{sat}_{\bar{\phi}_{T_i}}\Big(\hat{\phi}_{T_i}\Big)\Big).
\end{aligned} \tag{41}$$

According to (39), (40), and (41), we obtain

$$\begin{aligned}
\dot{\mathcal{V}}_r &\le \sum_{i=1}^{n}\frac{1}{2}\Big[\tilde{\phi}_i\Gamma_i^{-1}\tilde{\phi}_i - \Big(\phi_{T_i} - \text{sat}_{\bar{\phi}_{T_i}}\Big(\hat{\phi}_{T_i}\Big)\Big)\Gamma_i^{-1}\Big(\phi_{T_i} - \text{sat}_{\bar{\phi}_{T_i}}\Big(\hat{\phi}_{T_i}\Big)\Big)\Big] \\
&= \sum_{i=1}^{n}\frac{1}{2}\Big(2\phi_i\Gamma_i^{-1}\,\text{sat}_{\bar{\phi}_{T_i}}\Big(\hat{\phi}_{T_i}\Big) - 2\hat{\phi}_i\Gamma_i^{-1}\phi_i \\
&\qquad + \hat{\phi}_i\Gamma_i^{-1}\hat{\phi}_i - \text{sat}_{\bar{\phi}_{T_i}}\Big(\hat{\phi}_{T_i}\Big)\Gamma_i^{-1}\,\text{sat}_{\bar{\phi}_{T_i}}\Big(\hat{\phi}_{T_i}\Big) \\
&\qquad + 2\hat{\phi}_i\Gamma_i^{-1}\,\text{sat}_{\bar{\phi}_{T_i}}\Big(\hat{\phi}_{T_i}\Big) - 2\hat{\phi}_i\Gamma_i^{-1}\,\text{sat}_{\bar{\phi}_{T_i}}\Big(\hat{\phi}_{T_i}\Big)\Big) \\
&= \sum_{i=1}^{n} -\frac{1}{2}\Big[\hat{\phi}_i - \text{sat}_{\bar{\phi}_{T_i}}\Big(\hat{\phi}_{T_i}\Big)\Big] \times \Gamma_i^{-1}\Big[\hat{\phi}_i - \text{sat}_{\bar{\phi}_{T_i}}\Big(\hat{\phi}_{T_i}\Big)\Big] \\
&\quad - \sum_{i=1}^{n}\tilde{\phi}_i^T\Gamma_i^{-1}\Big[\hat{\phi}_i - \text{sat}_{\bar{\phi}_{T_i}}\Big(\hat{\phi}_{T_i}\Big)\Big].
\end{aligned} \tag{42}$$

Applying the learning law (35) in (42) yields

$$\dot{\mathcal{V}}_r \leq \sum_{i=1}^{n}\left(-\frac{1}{2}s_i(x)\Gamma_i s_i(x)\alpha_i^2 z_i^2\right) - \sum_{i=1}^{n}\left(\tilde{\phi}_i s_i(x) z_i \alpha_i\right) \tag{43}$$

which further indicates that

$$\sum_{i=1}^{n}\left(\tilde{\phi}_i s_i(x) z_i \alpha_{ii}\right) = z^T \alpha \tilde{\boldsymbol{\phi}}^T \boldsymbol{s}(\boldsymbol{x}). \tag{44}$$

Substituting (44) into (43), we have

$$\dot{\mathcal{V}}_r \leq -z^T \alpha \tilde{\boldsymbol{\phi}}^T \boldsymbol{s}(\boldsymbol{x}) + \sum_{i=1}^{n}\left(-\frac{1}{2}s_i(x)\Gamma_i s_i(x)\alpha_i^2 z_i^2\right). \tag{45}$$

Combining (36) and (45), by defining $\mathcal{V}_1 = \mathcal{V}_f + \mathcal{V}_r$, we can conclude that

$$\dot{\mathcal{V}}_1 \leq -z^T \kappa z - \frac{1}{2}\sum_{i=1}^{n}\left(s_i(x)\Gamma_i s_i(x)\alpha_i^2 z_i^2\right) + z^T \alpha \boldsymbol{Q_2}. \tag{46}$$

It can be seen from (46) that $\dot{\mathcal{V}}_1 \leq 0$ is not necessarily true because of $\boldsymbol{Q_2}$. Therefore, we need to design a controller to deal with $\boldsymbol{Q_2}$.

Remark 4: As discussed before, the repetitive learning control can deal with periodic disturbance. According to (35), the boundedness of $\hat{\boldsymbol{\phi}}$ is guaranteed, but $\hat{\boldsymbol{\phi}}$ cannot be constrained within a predefined region due to the unsaturated term in (35). Therefore, we investigate a fully saturation learning to address this problem and ensure that $\hat{\boldsymbol{\phi}}$ is within a known region. Finally, we use a disturbance observer to address $\boldsymbol{Q_2}$.

D. Adaptive Repetitive Control With Disturbance Observer

In order to obtain the full saturation learning law, we have to ensure that all items of the repeated learning law are constrained within a region. In this section, we propose a fully saturated learning law to learn periodic disturbances and prove that the closed-loop system is stable through the error convergence analysis. Given the adaptive weight matrix in (26), we have

$$\boldsymbol{H}(\boldsymbol{x}) = \hat{\boldsymbol{\beta}}^T \boldsymbol{w}(\boldsymbol{x}). \tag{47}$$

Consider the following adaptive repetitive controller:

$$\boldsymbol{\tau} = \boldsymbol{\tau_1} + \boldsymbol{\tau_2} \tag{48}$$

where $\boldsymbol{\tau_1} = -\alpha^{-1}\kappa z - \hat{\boldsymbol{\beta}}^T \boldsymbol{w}(\boldsymbol{x})$ and $\boldsymbol{\tau_2} = -\hat{\boldsymbol{\phi}}^T \boldsymbol{s}(\boldsymbol{x})$.

A fully saturated learning law is designed as

$$\hat{\phi}_i(t) = \begin{cases} \text{sat}_{\bar{\phi}_{e_i}}\left(\hat{\phi}_{e_i}(t)\right), & t > 0 \\ 0, & t \in [-T, 0] \end{cases} \tag{49}$$

where $\hat{\phi}_{e_i}(t) = \hat{\phi}_i(t-T) + \Gamma_i \alpha_i s_i(x) z_i$, $\bar{\boldsymbol{\phi}}_{\boldsymbol{e}} = \text{diag}[\bar{\phi}_{e_1}, \ldots, \bar{\phi}_{e_n}]$, $\hat{\boldsymbol{\phi}}_{\boldsymbol{e}} = \text{diag}[\hat{\phi}_{e_1}, \ldots, \hat{\phi}_{e_n}]$ and we define $\bar{\phi}_{e_i}$ as the lower and upper bounds of $\hat{\phi}_{e_i}$.

The following adaptive update law is designed as:

$$\dot{\hat{\boldsymbol{\beta}}}_{\boldsymbol{i}} = \Phi_i \alpha_i w_i(x) z_i - \Phi_i \varrho \hat{\boldsymbol{\beta}}_{\boldsymbol{i}} \tag{50}$$

where $\Phi_i \in \mathbb{R}^{l \times l} > 0$ is a diagonal matrix and ϱ is a positive constant.

In order to design an observer, we define an auxiliary variable

$$\boldsymbol{\mathcal{R}} = \boldsymbol{Q_2} - K_d \boldsymbol{x_2} \tag{51}$$

where $K_d \in \mathbb{R}^{n \times n}$ is a diagonal matrix. According to Assumption 2, we know that

$$||\dot{\boldsymbol{Q}}_{\boldsymbol{2}}|| \leq \epsilon_q \tag{52}$$

where ϵ_q is a positive constant. According to (17), the time derivative of $\boldsymbol{\mathcal{R}}$ in (51) is

$$\dot{\boldsymbol{\mathcal{R}}} = \dot{\boldsymbol{Q}}_{\boldsymbol{2}} - \boldsymbol{K_d M_d}^{-1}(\boldsymbol{P}(\boldsymbol{x}) + \boldsymbol{\tau} + \boldsymbol{Q_1} + \boldsymbol{Q_2}). \tag{53}$$

We use $\hat{\boldsymbol{Q}}_{\boldsymbol{2}}$ to represent the estimation of $\boldsymbol{Q_2}$ and define an estimation update law of $\boldsymbol{\mathcal{R}}$ as

$$\dot{\hat{\boldsymbol{\mathcal{R}}}} = -K_d \boldsymbol{M_d^{-1}}\left(\hat{\boldsymbol{\beta}}^T \boldsymbol{w}(\boldsymbol{x}) - \boldsymbol{h}(\boldsymbol{x}) + \boldsymbol{\tau} + \hat{\boldsymbol{\phi}}^T \boldsymbol{s}(\boldsymbol{x}) + \hat{\boldsymbol{Q}}_{\boldsymbol{2}}\right) \tag{54}$$

and we can obtain $\hat{\boldsymbol{Q}}_{\boldsymbol{2}}$ as

$$\hat{\boldsymbol{Q}}_{\boldsymbol{2}} = \hat{\boldsymbol{\mathcal{R}}} + K_d \boldsymbol{x_2}. \tag{55}$$

Finally, we can obtain the following controller with an observer:

$$\boldsymbol{\tau} = \boldsymbol{\tau_1} + \boldsymbol{\tau_2} - \hat{\boldsymbol{Q}}_{\boldsymbol{2}}. \tag{56}$$

$\tilde{\boldsymbol{Q}}_{\boldsymbol{2}} = \boldsymbol{Q_2} - \hat{\boldsymbol{Q}}_{\boldsymbol{2}}$ is the observation estimation error. According to (55), we have

$$\tilde{\boldsymbol{\mathcal{R}}} = \boldsymbol{\mathcal{R}} - \hat{\boldsymbol{\mathcal{R}}} = \tilde{\boldsymbol{Q}}_{\boldsymbol{2}}. \tag{57}$$

Hence, the derivative of $\tilde{\boldsymbol{Q}}_{\boldsymbol{2}}$ is

$$\begin{aligned}\dot{\tilde{\boldsymbol{Q}}}_{\boldsymbol{2}} &= \dot{\boldsymbol{\mathcal{R}}} - \dot{\hat{\boldsymbol{\mathcal{R}}}} \\ &= \dot{\boldsymbol{Q}}_{\boldsymbol{2}} + K_d \boldsymbol{M_d^{-1}}\left(-\tilde{\boldsymbol{\beta}}^T \boldsymbol{w}(\boldsymbol{x}) - \tilde{\boldsymbol{\phi}}^T \boldsymbol{s}(\boldsymbol{x}) - \tilde{\boldsymbol{Q}}_{\boldsymbol{2}}\right).\end{aligned} \tag{58}$$

Define $\mathcal{V}_q = \frac{1}{2}\tilde{\boldsymbol{Q}}_{\boldsymbol{2}}^T \tilde{\boldsymbol{Q}}_{\boldsymbol{2}}$, and its derivative is

$$\dot{\mathcal{V}}_q = \tilde{\boldsymbol{Q}}_{\boldsymbol{2}}^T \dot{\tilde{\boldsymbol{Q}}}_{\boldsymbol{2}} = \tilde{\boldsymbol{Q}}_{\boldsymbol{2}}^T\left(\dot{\boldsymbol{Q}}_{\boldsymbol{2}} - \dot{\hat{\boldsymbol{Q}}}_{\boldsymbol{2}}\right). \tag{59}$$

Substituting (58) into (59), we have

$$\dot{\mathcal{V}}_q = \tilde{\boldsymbol{Q}}_{\boldsymbol{2}}^T\left(\dot{\boldsymbol{Q}}_{\boldsymbol{2}} + K_d \boldsymbol{M_d^{-1}}\left(-\tilde{\boldsymbol{\beta}}^T \boldsymbol{w}(\boldsymbol{x}) - \tilde{\boldsymbol{\phi}}^T \boldsymbol{s}(\boldsymbol{x}) - \tilde{\boldsymbol{Q}}_{\boldsymbol{2}}\right)\right). \tag{60}$$

According to (52) and $\tilde{\boldsymbol{Q}}_{\boldsymbol{2}}^T \dot{\boldsymbol{Q}}_{\boldsymbol{2}} \leq ([\tilde{\boldsymbol{Q}}_{\boldsymbol{2}}^T \tilde{\boldsymbol{Q}}_{\boldsymbol{2}}]/2) + ([||\dot{\boldsymbol{Q}}_{\boldsymbol{2}}||^2]/2)$, we obtain

$$\begin{aligned}\dot{\mathcal{V}}_q \leq\ & \frac{\tilde{\boldsymbol{Q}}_{\boldsymbol{2}}^T \tilde{\boldsymbol{Q}}_{\boldsymbol{2}}}{2} + \frac{\epsilon_q^2}{2} - \tilde{\boldsymbol{Q}}_{\boldsymbol{2}}^T K_d \boldsymbol{M_d^{-1}} \tilde{\boldsymbol{\beta}}^T \boldsymbol{w}(\boldsymbol{x}) \\ & - \tilde{\boldsymbol{Q}}_{\boldsymbol{2}}^T K_d \boldsymbol{M_d^{-1}} \tilde{\boldsymbol{\phi}}^T \boldsymbol{s}(\boldsymbol{x}) - \tilde{\boldsymbol{Q}}_{\boldsymbol{2}}^T K_d \boldsymbol{M_d^{-1}} \tilde{\boldsymbol{Q}}_{\boldsymbol{2}}.\end{aligned} \tag{61}$$

Consider the following Lyapunov function candidate:

$$\mathcal{V}_a = \sum_{i=1}^{n} \frac{1}{2} \tilde{\boldsymbol{\beta}}_{\boldsymbol{i}}^T \Phi_i^{-1} \tilde{\boldsymbol{\beta}}_{\boldsymbol{i}} \tag{62}$$

where $\tilde{\boldsymbol{\beta}}_{\boldsymbol{i}} = \boldsymbol{\beta_i} - \hat{\boldsymbol{\beta}}_{\boldsymbol{i}}$. According to [43], and taking the time derivative of (62), we have

$$\begin{aligned}\dot{\mathcal{V}}_a &= -\sum_{i=1}^{n}\tilde{\boldsymbol{\beta}}_i^T\Phi_i^{-1}\dot{\hat{\boldsymbol{\beta}}}_i \\ &= -\sum_{i=1}^{n}\tilde{\boldsymbol{\beta}}_i^T\Phi_i^{-1}\left(\Phi_i\alpha_i w_i(x)z_i - \Phi_i\varrho\hat{\boldsymbol{\beta}}_i\right) \\ &= -\sum_{i=1}^{n}\tilde{\boldsymbol{\beta}}_i^T\alpha_i w_i(x)z_i + \sum_{i=1}^{n}\varrho\tilde{\boldsymbol{\beta}}_i^T\hat{\boldsymbol{\beta}}_i \\ &= -z^T\alpha\tilde{\boldsymbol{\beta}}^T\boldsymbol{w}(\boldsymbol{x}) + \sum_{i=1}^{n}\varrho\tilde{\boldsymbol{\beta}}_i^T\left(\boldsymbol{\beta}_i - \tilde{\boldsymbol{\beta}}_i\right) \\ &\le -z^T\alpha\tilde{\boldsymbol{\beta}}^T\boldsymbol{w}(\boldsymbol{x}) + \sum_{i=1}^{n}\varrho\left(\frac{||\tilde{\boldsymbol{\beta}}_i||^2}{2} + \frac{||\boldsymbol{\beta}_i||^2}{2} - ||\tilde{\boldsymbol{\beta}}_i||^2\right) \\ &= -z^T\alpha\tilde{\boldsymbol{\beta}}^T\boldsymbol{w}(\boldsymbol{x}) + \sum_{i=1}^{n}\varrho\left(-\frac{||\tilde{\boldsymbol{\beta}}_i||^2}{2} + \frac{||\boldsymbol{\beta}_i||^2}{2}\right). \end{aligned} \tag{63}$$

Let $\mathcal{V}_r(t) = (1/2)\ \sum_{i=1}^{n}\int_{t-T}^{t}\tilde{\phi}_i(\tau)\Gamma_i^{-1}\tilde{\phi}_i(\tau)d\tau$. We have

$$\begin{aligned}\dot{\mathcal{V}}_r &= \sum_{i=1}^{n}\frac{1}{2}\left[\tilde{\phi}_i\Gamma_i^{-1}\tilde{\phi}_i - \left(\phi_{T_i} - \hat{\phi}_{T_i}\right)\Gamma_i^{-1}\left(\phi_{T_i} - \hat{\phi}_{T_i}\right)\right] \\ &= \frac{1}{2}\sum_{i=1}^{n}\Big(-2\phi_i\Gamma_i^{-1}\hat{\phi}_i + \hat{\phi}_i\Gamma_i^{-1}\hat{\phi}_i \\ &\qquad + 2\phi_{T_i}\Gamma_i^{-1}\hat{\phi}_{T_i} - \hat{\phi}_{T_i}\Gamma_i^{-1}\hat{\phi}_{T_i}\Big) \\ &= \frac{1}{2}\sum_{i=1}^{n}\Big(-2\phi_i\Gamma_i^{-1}\hat{\phi}_i + \hat{\phi}_i\Gamma_i^{-1}\hat{\phi}_i + 2\phi_{T_i}\Gamma_i^{-1}\hat{\phi}_{T_i} \\ &\qquad + \hat{\phi}_{T_i}\Gamma_i^{-1}\hat{\phi}_i - \hat{\phi}_i\Gamma_i^{-1}\hat{\phi}_{T_i} - \hat{\phi}_{T_i}\Gamma_i^{-1}\hat{\phi}_{T_i}\Big) \\ &= \sum_{i=1}^{n} -\tilde{\phi}_i\Gamma_i^{-1}\left[\hat{\phi}_i - \hat{\phi}_{T_i}\right] - \sum_{i=1}^{n}\frac{1}{2}\left[\hat{\phi}_i - \hat{\phi}_{T_i}\right]\Gamma_i^{-1}\left[\hat{\phi}_i - \hat{\phi}_{T_i}\right]. \end{aligned} \tag{64}$$

By applying the learning law (49) to (64), we have

$$\begin{aligned}\dot{\mathcal{V}}_r &= \sum_{i=1}^{n}\left[\phi_i(t) - \mathrm{sat}_{\bar{\phi}_{e_i}}\left(\hat{\phi}_{e_i}\right)\right]\Gamma_i^{-1} \\ &\quad\times\left[\hat{\phi}_{e_i} - \mathrm{sat}_{\bar{\phi}_{e_i}}\left(\hat{\phi}_{e_i}\right) - \Gamma_i\alpha_i s_i(x)z_i\right] \\ &\quad - \sum_{i=1}^{n}\frac{1}{2}\left[\hat{\phi}_i - \hat{\phi}_{T_i}\right]\Gamma_i^{-1}\left[\hat{\phi}_i - \hat{\phi}_{T_i}\right] \\ &= \sum_{i=1}^{n}\left[\phi_i - \mathrm{sat}_{\bar{\phi}_{e_i}}\left(\hat{\phi}_{e_i}\right)\right]\Gamma_i^{-1}\times\left[\hat{\phi}_{e_i} - \mathrm{sat}_{\bar{\phi}_{e_i}}\left(\hat{\phi}_{e_i}\right)\right] \\ &\quad - \sum_{i=1}^{n}\tilde{\phi}_i\alpha_i s_i(x(t))z_i - \sum_{i=1}^{n}\frac{1}{2}\left[\hat{\phi}_i - \hat{\phi}_{T_i}\right]\Gamma_i^{-1}\left[\hat{\phi}_i(t) - \hat{\phi}_{T_i}\right] \\ &= \sum_{i=1}^{n}\left[\phi_i - \mathrm{sat}_{\bar{\phi}_{e_i}}\left(\hat{\phi}_{e_i}\right)\right]\Gamma_i^{-1}\times\left[\hat{\phi}_{e_i}(t) - \mathrm{sat}_{\bar{\phi}_{e_i}}\left(\hat{\phi}_{e_i}(t)\right)\right] \\ &\quad - z^T\alpha\tilde{\boldsymbol{\phi}}^T\boldsymbol{s}(\boldsymbol{x}) - \sum_{i=1}^{n}\frac{1}{2}\left[\hat{\phi}_i - \hat{\phi}_{T_i}\right]\Gamma_i^{-1}\left[\hat{\phi}_i - \hat{\phi}_{T_i}\right]. \end{aligned} \tag{65}$$

By Lemma 2, for the case $\gamma = 0$, $[\phi_i(t) - \mathrm{sat}_{\bar{\phi}_{e_i}}(\hat{\phi}_{e_i}(t))]\Gamma_i^{-1}[\hat{\phi}_{e_i}(t) - \mathrm{sat}_{\bar{\phi}_{e_i}}(\hat{\phi}_{e_i}(t))] \le 0$, which results in

$$\dot{V}_r \le -z^T\alpha\tilde{\boldsymbol{\phi}}^T\boldsymbol{s}(\boldsymbol{x}) - \frac{1}{2}\sum_{i=1}^{n}\left[\hat{\phi}_i - \hat{\phi}_{T_i}\right]\Gamma_i^{-1}\left[\hat{\phi}_i - \hat{\phi}_{T_i}\right]. \tag{66}$$

Consider the augmented Lyapunov function candidate

$$\mathcal{V}_2 = \mathcal{V}_f + \mathcal{V}_r + \mathcal{V}_a + \mathcal{V}_q. \tag{67}$$

The time derivative of $\mathcal{V}_2$ is

$$\dot{\mathcal{V}}_2 = \dot{\mathcal{V}}_f + \dot{\mathcal{V}}_r + \dot{\mathcal{V}}_a + \dot{\mathcal{V}}_q. \tag{68}$$

Substituting (56) into (28) yields

$$\begin{aligned}\dot{\mathcal{V}}_f &= z^T\alpha\left[\boldsymbol{\beta}^T\boldsymbol{w}(\boldsymbol{x}) + \boldsymbol{Q} + \hat{\boldsymbol{\tau}}_f + \hat{\boldsymbol{\tau}}_r - \hat{\boldsymbol{Q}}_2\right] \\ &= z^T\alpha\Big[\boldsymbol{\beta}^T\boldsymbol{w}(\boldsymbol{x}) + \boldsymbol{Q} - \alpha^{-1}\kappa z \\ &\qquad - \hat{\boldsymbol{\beta}}^T\boldsymbol{w}(\boldsymbol{x}) - \hat{\boldsymbol{\phi}}^T\boldsymbol{s}(\boldsymbol{x}) - \hat{\boldsymbol{Q}}_2\Big] \\ &= z^T\alpha\left[\tilde{\boldsymbol{\beta}}^T\boldsymbol{w}(\boldsymbol{x}) + \tilde{\boldsymbol{\phi}}^T\boldsymbol{s}(\boldsymbol{x}) - \alpha^{-1}\kappa z + \tilde{\boldsymbol{Q}}_2\right] \\ &= -z^T\kappa z + z^T\alpha\tilde{\boldsymbol{\beta}}^T\boldsymbol{w}(\boldsymbol{x}) + z^T\alpha\tilde{\boldsymbol{\phi}}^T\boldsymbol{s}(\boldsymbol{x}) + z^T\alpha\tilde{\boldsymbol{Q}}_2. \end{aligned} \tag{69}$$

Because $w(x)$ represents a regress vector and $s(x)$ is a saturation function vector, we have $||w(x)|| \le \epsilon_w$ and $||s(x)|| \le \epsilon_s$. Combining (61), (63), (65), (68), (69), $-\tilde{\boldsymbol{Q}}_2^T K_d\boldsymbol{M}_d^{-1}\tilde{\boldsymbol{\beta}}^T\boldsymbol{w}(\boldsymbol{x}) \le ([\tilde{\boldsymbol{Q}}_2^T\tilde{\boldsymbol{Q}}_2]/2) + ([||K_d\boldsymbol{M}_d^{-1}||^2\epsilon_w^2||\tilde{\boldsymbol{\beta}}||^2]/2)$, $-\tilde{\boldsymbol{Q}}_2^T K_d\boldsymbol{M}_d^{-1}\tilde{\boldsymbol{\phi}}^T\boldsymbol{s}(\boldsymbol{x}) \le ([\tilde{\boldsymbol{Q}}_2^T\tilde{\boldsymbol{Q}}_2]/2) + ([||K_d\boldsymbol{M}_d^{-1}||^2\epsilon_s^2||\tilde{\boldsymbol{\phi}}||^2]/2)$, and $z^T\alpha\tilde{\boldsymbol{Q}}_2 \le ([z^T\alpha\alpha z]/2) + ([\tilde{\boldsymbol{Q}}_2^T\tilde{\boldsymbol{Q}}_2]/2)$, we have

$$\begin{aligned}\dot{\mathcal{V}}_2 &\le -z^T\kappa z + z^T\alpha\tilde{\boldsymbol{\beta}}^T\boldsymbol{w}(\boldsymbol{x}) + z^T\alpha\tilde{\boldsymbol{\phi}}^T\boldsymbol{s}(\boldsymbol{x}) \\ &\quad - z^T\alpha\tilde{\boldsymbol{\phi}}^T\boldsymbol{s}(\boldsymbol{x}) - \frac{1}{2}\sum_{i=1}^{n}\left[\hat{\phi}_i - \hat{\phi}_{T_i}\right]\Gamma_i^{-1}\left[\hat{\phi}_i - \hat{\phi}_{T_i}\right] \\ &\quad - z^T\alpha\tilde{\boldsymbol{\beta}}^T\boldsymbol{w}(\boldsymbol{x}) + \sum_{i=1}^{n}\varrho\left(\frac{||\boldsymbol{\beta}_i||^2}{2} - \frac{||\tilde{\boldsymbol{\beta}}_i||^2}{2}\right) \\ &\quad + z^T\alpha\tilde{\boldsymbol{Q}}_2 + \frac{\tilde{\boldsymbol{Q}}_2^T\tilde{\boldsymbol{Q}}_2}{2} + \frac{\epsilon_q^2}{2} - \tilde{\boldsymbol{Q}}_2^T K_d\boldsymbol{M}_d^{-1}\tilde{\boldsymbol{\beta}}^T\boldsymbol{w}(\boldsymbol{x}) \\ &\quad - \tilde{\boldsymbol{Q}}_2^T K_d\boldsymbol{M}_d^{-1}\tilde{\boldsymbol{\phi}}^T\boldsymbol{s}(\boldsymbol{x}) - \tilde{\boldsymbol{Q}}_2^T K_d\boldsymbol{M}_d^{-1}\tilde{\boldsymbol{Q}}_2 \\ &\le -z^T\kappa z - \frac{1}{2}\sum_{i=1}^{n}\left[\hat{\phi}_i - \hat{\phi}_{T_i}\right]\Gamma_i^{-1}\left[\hat{\phi}_i - \hat{\phi}_{T_i}\right] \\ &\quad + \sum_{i=1}^{n}\varrho\left(\frac{||\boldsymbol{\beta}_i||^2}{2} - \frac{||\tilde{\boldsymbol{\beta}}_i||^2}{2}\right) \\ &\quad + \frac{z^T\alpha\alpha z}{2} + \frac{\tilde{\boldsymbol{Q}}_2^T\tilde{\boldsymbol{Q}}_2}{2} + \frac{\tilde{\boldsymbol{Q}}_2^T\tilde{\boldsymbol{Q}}_2}{2} + \frac{\epsilon_q^2}{2} \\ &\quad + \frac{\tilde{\boldsymbol{Q}}_2^T\tilde{\boldsymbol{Q}}_2}{2} + \frac{||K_d\boldsymbol{M}_d^{-1}||^2\epsilon_w^2||\tilde{\boldsymbol{\beta}}||^2}{2} + \frac{\tilde{\boldsymbol{Q}}_2^T\tilde{\boldsymbol{Q}}_2}{2} \\ &\quad + \frac{||K_d\boldsymbol{M}_d^{-1}||^2\epsilon_s^2||\tilde{\boldsymbol{\phi}}||^2}{2} - \tilde{\boldsymbol{Q}}_2^T K_d\boldsymbol{M}_d^{-1}\tilde{\boldsymbol{Q}}_2. \end{aligned} \tag{70}$$

Considering that $\hat{\phi}_i$ is a saturated variable, we have $|\tilde{\phi}_i| = |\phi_i - \hat{\phi}_i| \le 2\bar{\phi}$. Hence, $||\tilde{\boldsymbol{\phi}}||^2 \le \sum_{i=1}^{n}(2\bar{\phi}) = 4n\bar{\phi}^2$. Equation (70) can thus be rewritten as

$$\begin{aligned}\dot{\mathcal{V}}_2 &\le -z^T\left(\kappa - \frac{\alpha\alpha}{2}\right)z - \tilde{\boldsymbol{Q}}_2^T\left(K_d\boldsymbol{M}_d^{-1} - 2I\right)\tilde{\boldsymbol{Q}}_2 \\ &\quad - \frac{\varrho - ||K_d\boldsymbol{M}_d^{-1}||^2\epsilon_w^2}{2}\sum_{i=1}^{n}\tilde{\boldsymbol{\beta}}_i{}^T\tilde{\boldsymbol{\beta}}_i + \epsilon \\ &\le -z^T\left(\kappa - \frac{\alpha\alpha}{2}\right)z + \epsilon \end{aligned} \tag{71}$$

where $\epsilon = (\epsilon_q^2/2) + ([4||K_d\boldsymbol{M_d^{-1}}||^2\epsilon_s^2 n\bar{\phi}^2]/2) + \sum_{i=1}^{n}\varrho(||\boldsymbol{\beta_i}||^2/2)$. Because $\boldsymbol{\beta_i}$ represents the optimal weight and $||\boldsymbol{\beta_i}||^2$ is also a bounded value.

We define the minimum eigenvalue of $(\kappa - [\alpha\alpha/2])$ as $\check{\lambda}^a$. From (71), we have

$$\dot{\mathcal{V}}_2 \leq -\check{\lambda}^a \boldsymbol{z}^T\boldsymbol{z} + \epsilon. \tag{72}$$

Thus, $\dot{\mathcal{V}}_2 < 0$ is achieved outside the region $\{z|\boldsymbol{z}^T\boldsymbol{z} \leq (\epsilon/\check{\lambda}^a)\}$. So, $\boldsymbol{z}$ is ultimately bounded with

$$\lim_{t\to\infty} ||z|| \in \left[-\sqrt{\frac{\epsilon}{\check{\lambda}^a}}, \sqrt{\frac{\epsilon}{\check{\lambda}^a}}\right]. \tag{73}$$

Equations (72) and (73) imply that $\mathcal{V}_2(t) \leq 0$ outside a compact set, which follows that all signals in the closed-loop system in (14) are bounded.

IV. Experimental Verification

In order to verify the effectiveness of our trajectory planning method and the tracking performance of adaptive repetitive controller, a healthy subject (male, 24 years old, height 178 cm, weight 73 kg) participates as a volunteer. The participant is required to wear the exoskeleton and walk forward for about 50 s. To further test its performance for the elder or patients, the participant is required to use a crutch during walking.

We have developed a walking exoskeleton for experiments, which has two passive degrees of freedom (DOFs) and eight active DOFs. Its hip joint has a pitch DOF, a roll DOF, and a yaw DOF, respectively. Its knee has one pitch DOF, and its ankle has one passive DOF. The pitch DOF indicates that the pitch joint of exoskeleton can perform flexion and extension, the yaw DOF means that the yaw joint of an exoskeleton can perform rotation, and the roll DOF enables the roll joint of exoskeleton to perform adduction and abduction. Its hip can perform flexion, extension, rotation outside and inside, adduction, and abduction. The ankle joint can perform dorsiflexion and plantar flexion as a passive DOF. In addition, the length of the hip is 0.485 m, the length of the foot is 0.275 m, and the width is 0.125 m in our designed walking exoskeleton.

The hardware devices of our wearable walking exoskeleton mainly includes a computer, some sensors, and motors. The eight active joints are driven by a Maxon DC servo motor with an incremental encoder. Each motor has a 160:1 harmonic transmission and a maximum speed of 5000 r/min. We adopt four Copley motion drivers to drive the above eight Maxon motors and the Copley motion drivers can communicate with a host computer via a EtherCAT communication protocol. The host computer as our processing platform runs a real-time operating system, and its sampling interval of the motion control engine is 1 ms.

A. Experimental Setting and Design

Before the experiment, the desired joint angle trajectory is generated based on our exoskeleton model using DCM mentioned in Section II. Considering a dynamic walking of exoskeleton in sagittal plane and vertical plane, we have six active joints for trajectory planning, that is, $n = 6$, and these six joints are left hip pitch joint, left knee pitch joint, right hip pitch joint, right knee pitch joint, right hip roll joint, and left hip roll joint, respectively. In addition, MATLAB 2018a is used to generate the desired trajectory. The mechanical parameters related to exoskeleton we used are designed as $h = 0.73$ m, and the gravitational constant is set as $g = 9.8$ m/s^2 in trajectory planning. The parameter dT is selected as 1.3 s, and the total time for smooth transition is chosen as $T_t = 0.26$ s. As shown in Fig. 4, the exoskeleton starts to walk forward initially from an initial standing state. Once an initial walking step is completed, exoskeleton starts to take the first whole step, and then repeats the movement of the first whole step in the next walk. Hence, when planing the joint angle trajectory of exoskeleton, we divide the joint angle trajectory planning into two stages. The first stage is the initial walking, and the parameters are designed as $T_S = 0.65$ s, $t_X = (T_S/1.4)$ s, $L_s = 0.33$ m, $h_f = 0.05$ m, and $t_Z = (T_S/1.5)$. The second stage consists of repetitive movement of an exoskeleton walking, and the single step cycle parameter is selected as $T_S = 1.3$ s, so the whole step cycle is $2 * T_S = 2.6$ s. Other parameters are designed as $t_X = (T_S/1.4)$ s, $L_s = 0.66$ m, $h_f = 0.05$ m, and $t_Z = (T_S/1.5)$. Considering the scenario of helping patients with neuro musculoskeletal stroke, we can obtain a step cycle time suitable for patients by stretching the time axis in the time domain without modifying the trajectory amplitude in the spatial dimension [45]. In this experiment, to assist patients to walk appropriately, we stretch the planned trajectory by a factor of two.

For the planned joint angle trajectory, the adaptive repetitive control is applied to track the trajectory. The parameters related to the controller are chosen as follows: $\Lambda = \text{diag}[420, 500, 420, 550, 400, 400]$, $\kappa = \text{diag}[0.05, 0.02, 0.05, 0.02, 0.1, 0.1]$, $\Phi_i = 5I$, $\alpha = 0.1I_{6\times6}$, $\Gamma = 2.2I_{6\times6}$, $K_d = 0.0025I_{6\times6}$, and $\boldsymbol{M_d} = 0.001\text{diag}[1 + 0.1\sin(q_2), 1 + 0.1\cos(q_1), 1 + 0.1\sin(q_4), 0.2(1 + 0.1\cos(q_3)), 1 + 0.1\sin(q_6), 1 + 0.1\cos(q_5)]$. The selected saturated function is $s(x(t)) = (t/1 + |t|)$, and $\overline{\phi}_{e_i} = \{-1, 1\}$. A method based on neural network is used in this article, the number of nodes is set as 256, the basis function $w_i(x)$ is selected as the Gaussian function, the variance is set as 10, $\hat{\boldsymbol{\beta}}_{\boldsymbol{i}}$ is initialized to 0.000001, and the input variable is chosen as $[\boldsymbol{q_d}, \boldsymbol{q}, \dot{\boldsymbol{q}}_{\boldsymbol{d}}, \dot{\boldsymbol{q}}]$.

B. Results and Analysis

The adaptive repetitive control strategy is used to track the generated trajectories in the experiments. As shown by the red line in Figs. 7–9, according to the mechanical structure and parameters of the exoskeleton and the proposed dynamics walking desired trajectory planning method, we can generate an effective desired trajectory. The walking experiment shows that the generated trajectory is suitable for the walking exoskeleton. In the adaptive repetitive control strategy, the fully saturated learning controller is designed to deal with disturbance. The tracking performance is shown in Figs. 7–9. From Figs. 7–9, we can observe that for the joint trajectories obtained based on DCM, our proposed adaptive repetitive

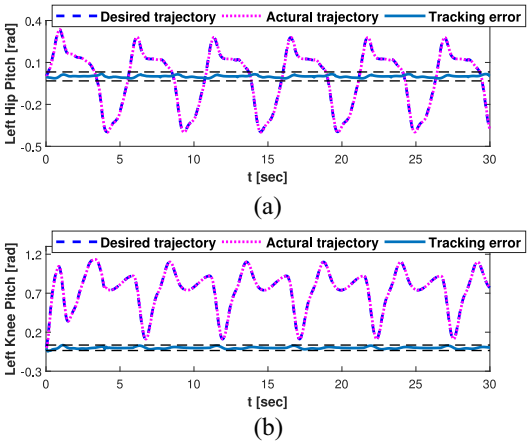

Fig. 7. Joint trajectory and the tracking error of left hip pitch and left knee pitch. Trajectory tracking results of (a) left hip pitch and (b) left knee pitch.

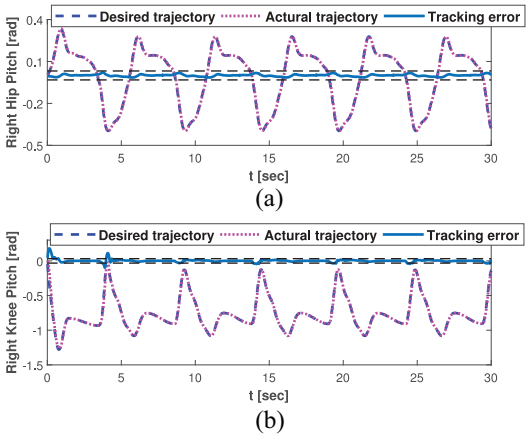

Fig. 8. Joint trajectory and the tracking error of right hip pitch and right knee pitch. Trajectory tracking results of (a) right hip pitch and (b) right knee pitch.

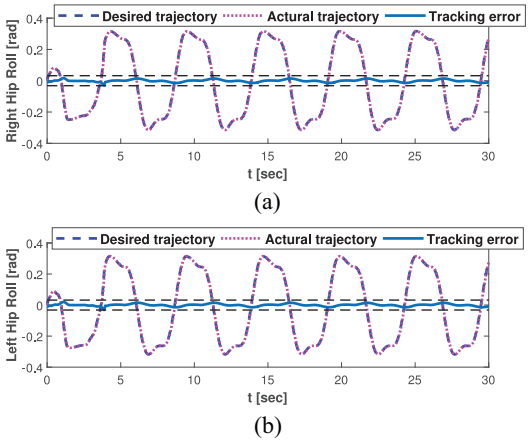

Fig. 9. Joint trajectory and the tracking error of left hip roll and right hip roll. Trajectory tracking results of (a) right hip roll and (b) left hip roll.

controller can effectively track them, and the position tracking errors of six joints are all converged to a bounded range. Fig. 10 shows the control input of each joint in this walking experiment, which indicates that the control input of each joint is bounded. Figs. 11 and 12 show the control input of fully saturated learning. Finally, the update laws of the fully

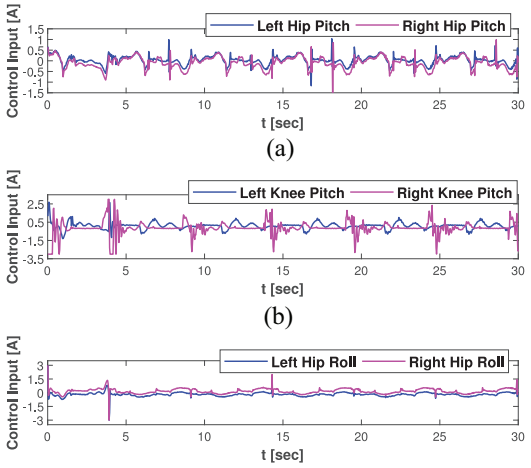

Fig. 10. Control input of left hip pitch, left knee pitch, left hip roll, right hip pitch, right knee pitch and right hip roll. (a) Left hip pitch and right hip pitch. (b) Left knee pitch and right knee pitch. (c) Left hip roll and right hip roll.

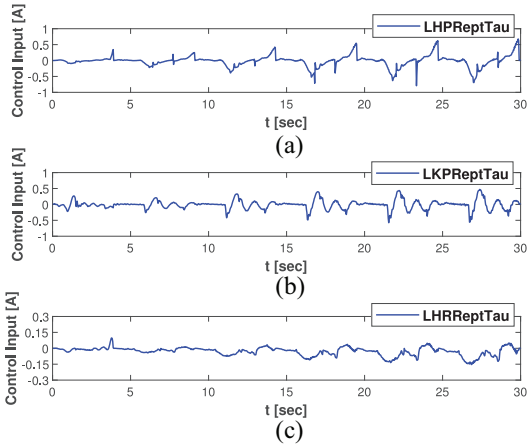

Fig. 11. Fully saturated learning control input of the left leg joint. (a) Left hip pitch. (b) Left knee pitch. (c) Left hip roll.

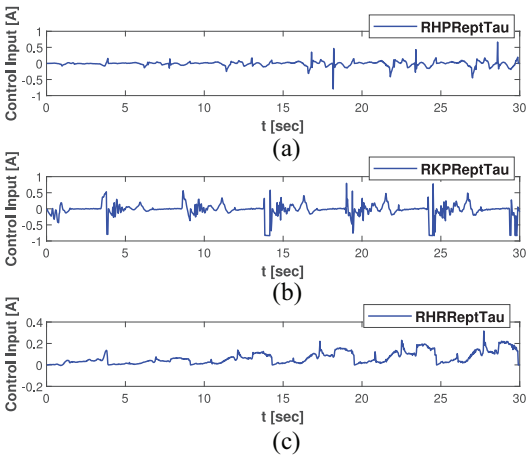

Fig. 12. Fully saturated learning control input of the right leg joint. (a) Right hip pitch. (b) Right knee pitch. (c) Right hip roll.

saturated learning are shown in Figs. 13 and 14, which indicates that the fully saturated learning laws change gradually in each step cycle and show a trend of gradual saturation of their

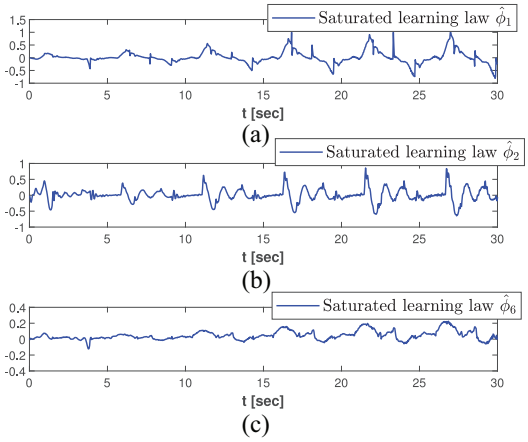

Fig. 13. Saturated learning laws (a) $\hat{\phi}_1$, (b) $\hat{\phi}_2$, and (c) $\hat{\phi}_6$.

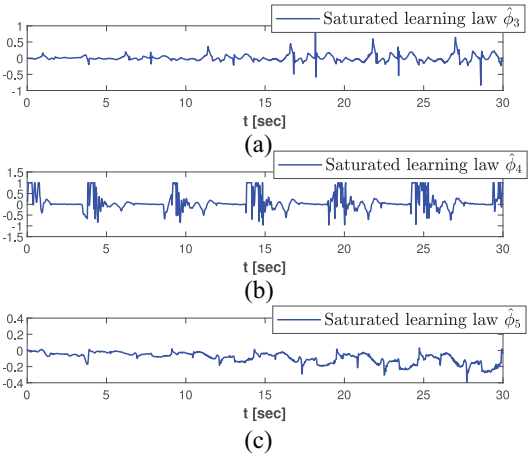

Fig. 14. Saturated learning laws (a) $\hat{\phi}_3$, (b) $\hat{\phi}_4$, and (c) $\hat{\phi}_5$.

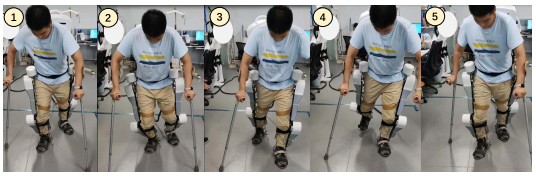

Fig. 15. Walking snapshots in a walking experiment.

values over time. Some walking snapshots during the walking experiment are shown in Fig. 15. The experimental results in this study demonstrate that our proposed walking trajectory planning method and adaptive repetitive control strategy for a walking exoskeleton are effective.

Finally, in order to further evaluate the tracking performance of our proposed controller, two performance indexes are used. They are mean absolute error (MAE) and root mean square error (RMSE). A proportional differential (PD) controller is widely used in robot control [46], [47]. Thus, we use it to compare with our proposed control strategy. The PD controller used in the experiment is $\boldsymbol{\tau} = -K_{cp}\boldsymbol{e} - K_{cd}\dot{\boldsymbol{e}}$ with $K_{cp} = \text{diag}[250, 80, 250, 60, 250, 250]$ and $K_{cd} = \text{diag}[0.5, 0.6, 0.5, 0.2, 1, 1]$. The comparison result is listed in Fig. 16, where LHP, LKP, LHR, RHP, RKP, and RHR represents left hip pitch, left knee pitch, left hip roll, right hip pitch,

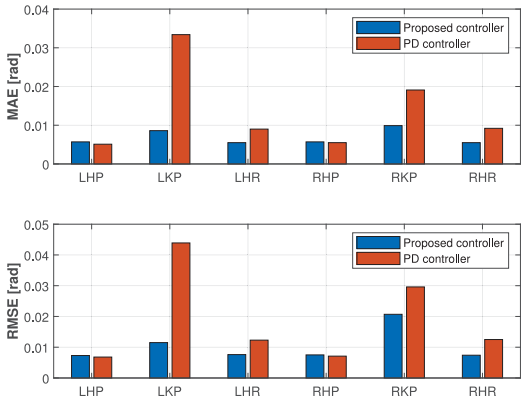

Fig. 16. Results of comparison with PD controller.

right knee pitch, and right hip roll, respectively. As exemplified in Fig. 16, the tracking performance between the proposed control strategy and PD controller is similar for LHP and RHP. However, for other joints, the proposed control strategy has a better tracking performance than the PD controller.

V. Conclusion

This work proposes a walking planning method and an adaptive repetitive control strategy for a walking exoskeleton to help patients with neuro musculoskeletal stroke. The trajectory of COM is obtained based on the relationship between COM and DCM. The trajectory of the ankle joint of an exoskeleton is then generated according to the trajectories of COM and ankle joint, which is translated to joint angles using the inverse kinematics of the robot. To deal with model uncertainties, a learning-based solution is developed to compensate for uncertainties. To deal with periodic disturbances, a fully saturated learning controller is designed to achieve bounded tracking performance. Extensive experiments are conducted to verify the effectiveness of the proposed walking planning method and the adaptive repetitive control strategy. The walking experimental results show that the developed trajectory planning method is effective and the proposed adaptive repetitive controller can efficiently deal with model uncertainties and periodic disturbances.

Although the proposed motion planning method can plan a walking trajectory for a walking exoskeleton, and the proposed adaptive repetitive learning controller can effectively track the trajectory of the exoskeleton, this method has some limitations. First, we plan the trajectory of the exoskeleton according to the coupling relationship among DCM, ZMP, and COM. Since ZMP is used in legged robots, our motion planning method may only be applied to legged robots, such as exoskeleton robots and quadruped robots. Second, the saturated learning controller proposed by us is aimed at periodic trajectory. Thus, we need to use another controller to deal with nonperiodic time-varying one. Our next work expects to further improve the motion planning method. We hope to apply it to quadruped robots. The motion planning scenario should include going straight and turning to an arbitrary direction [48], [49]. In

addition, we can try to improve the saturated learning controller to enable our proposed adaptive repetitive controller to track more complex trajectories.

REFERENCES

[1] W. Sun, J.-W. Lin, S.-F. Su, N. Wang, and M. J. Er, "Reduced adaptive fuzzy decoupling control for lower limb exoskeleton," *IEEE Trans. Cybern.*, vol. 51, no. 3, pp. 1099–1109, Mar. 2021.

[2] S. Pancholi, A. Giri, A. Jain, L. Kumar, and S. Roy, "Source aware deep learning framework for hand kinematic reconstruction using EEG signal," *IEEE Trans. Cybern.*, early access, May 9, 2022, doi: 10.1109/TCYB.2022.3166604.

[3] Y. Eguchi, H. Kadone, and K. Suzuki, "Standing mobility device with passive lower limb exoskeleton for upright locomotion," *IEEE/ASME Trans. Mechatronics*, vol. 23, no. 4, pp. 1608–1618, Aug. 2018.

[4] C. Zou, R. Huang, J. Qiu, Q. Chen, and H. Cheng, "Slope gradient adaptive gait planning for walking assistance lower limb exoskeletons," *IEEE Trans. Autom. Sci. Eng.*, vol. 18, no. 2, pp. 405–413, Apr. 2021.

[5] I. Farkhatdinov, J. Ebert, G. van Oort, M. Vlutters, E. van Asseldonk, and E. Burdet, "Assisting human balance in standing with a robotic exoskeleton," *IEEE Robot. Autom. Lett.*, vol. 4, no. 2, pp. 414–421, Apr. 2019.

[6] Y. Cao and J. Huang, "Neural-network-based nonlinear model predictive tracking control of a pneumatic muscle actuator-driven exoskeleton," *IEEE/CAA J. Automatica Sinica*, vol. 7, no. 6, pp. 1478–1488, Nov. 2020.

[7] T. Kamioka, H. Kaneko, T. Takenaka, and T. Yoshiike, "Simultaneous optimization of ZMP and footsteps based on the analytical solution of divergent component of motion," in *Proc. IEEE Int. Conf. Robot. Autom.*, 2018, pp. 1763–1770.

[8] M. Shafiee-Ashtiani, A. Yousefi-Koma, and M. Shariat-Panahi, "Robust bipedal locomotion control based on model predictive control and divergent component of motion," in *Proc. IEEE Int. Conf. Robot. Autom.*, 2017, pp. 3505–3510.

[9] M. A. Hopkins, D. W. Hong, and A. Leonessa, "Humanoid locomotion on uneven terrain using the time-varying divergent component of motion," in *Proc. IEEE-RAS Int. Conf. Humanoid Robots*, 2014, pp. 266–272.

[10] J. Englsberger, C. Ott, and A. Albu-Schäffer, "Three-dimensional bipedal walking control based on divergent component of motion," *IEEE Trans. Robot.*, vol. 31, no. 2, pp. 355–368, Apr. 2015.

[11] H. Jeong, I. Lee, J. Oh, K. K. Lee, and J.-H. Oh, "A robust walking controller based on online optimization of ankle, hip, and stepping strategies," *IEEE Trans. Robot.*, vol. 35, no. 6, pp. 1367–1386, Dec. 2019.

[12] Z. Li, T. Zhang, P. Huang, and G. Li, "Human-in-the-loop cooperative control of a walking exoskeleton for following time-variable human intention," *IEEE Trans. Cybern.*, early access, Oct. 25, 2022, doi: 10.1109/TCYB.2022.3211925.

[13] Y. Wen, J. Si, A. Brandt, X. Gao, and H. H. Huang, "Online reinforcement learning control for the personalization of a robotic knee prosthesis," *IEEE Trans. Cybern.*, vol. 50, no. 6, pp. 2346–2356, Jun. 2020.

[14] Z. Li, G. Li, X. Wu, Z. Kan, H. Su, and Y. Liu, "Asymmetric cooperation control of dual-arm exoskeletons using human collaborative manipulation models," *IEEE Trans. Cybern.*, vol. 52, no. 11, pp. 12126–12139, Nov. 2022.

[15] A. Martínez, B. Lawson, C. Durrough, and M. Goldfarb, "A velocity-field-based controller for assisting leg movement during walking with a bilateral hip and knee lower limb exoskeleton," *IEEE Trans. Robot.*, vol. 35, no. 2, pp. 307–316, Apr. 2019.

[16] Z. Li, Z. Ren, K. Zhao, C. Deng, and Y. Feng, "Human-cooperative control design of a walking exoskeleton for body weight support," *IEEE Trans. Ind. Informat.*, vol. 16, no. 5, pp. 2985–2996, May 2020.

[17] H. Xia, M. A. Khan, Z. Li, and M. Zhou, "Wearable robots for human underwater movement ability enhancement: A survey," *IEEE/CAA J. Automatica Sinica*, vol. 9, no. 6, pp. 967–977, Jun. 2022.

[18] R. Wu, Z. Yao, J. Si, and H. H. Huang, "Robotic knee tracking control to mimic the intact human knee profile based on actor–critic reinforcement learning," *IEEE/CAA J. Automatica Sinica*, vol. 9, no. 1, pp. 19–30, Jan. 2022.

[19] H. Huang, C. Yang, and C. L. P. Chen, "Optimal robot–environment interaction under broad fuzzy neural adaptive control," *IEEE Trans. Cybern.*, vol. 51, no. 7, pp. 3824–3835, Jul. 2021.

[20] B. Zhao, D. Liu, and C. Alippi, "Sliding-mode surface-based approximate optimal control for uncertain nonlinear systems with asymptotically stable critic structure," *IEEE Trans. Cybern.*, vol. 51, no. 6, pp. 2858–2869, Jun. 2021.

[21] H.-G. Han, Z. Liu, W. Lu, Y. Hou, and J.-F. Qiao, "Dynamic MOPSO-based optimal control for wastewater treatment process," *IEEE Trans. Cybern.*, vol. 51, no. 5, pp. 2518–2528, May 2021.

[22] T. Inoue, M. Nakano, and S. Iwai, "High accuracy control of servomechanism for repeated contouring," in *Proc. 10th Annu. Symp. Incremental Motion Contr. Syst. Devices*, 1981, pp. 282–292.

[23] M. Sun, S. S. Ge, and I. M. Y. Mareels, "Adaptive repetitive learning control of robotic manipulators without the requirement for initial repositioning," *IEEE Trans. Robot.*, vol. 22, no. 3, pp. 563–568, Jun. 2006.

[24] S. Li, M. Zhou, and X. Luo, "Modified primal-dual neural networks for motion control of redundant manipulators with dynamic rejection of harmonic noises," *IEEE Trans. Neural Netw. Learn. Syst.*, vol. 29, no. 10, pp. 4791–4801, Oct. 2018.

[25] Q. Chen, X. Yu, M. Sun, C. Wu, and Z. Fu, "Adaptive repetitive learning control of PMSM servo systems with bounded nonparametric uncertainties: Theory and experiments," *IEEE Trans. Ind. Electron.*, vol. 68, no. 9, pp. 8626–8635, Sep. 2021.

[26] C. M. Verrelli, S. Pirozzi, P. Tomei, and C. Natale, "Linear repetitive learning controls for robotic manipulators by Padé approximants," *IEEE Trans. Control Syst. Technol.*, vol. 23, no. 5, pp. 2063–2070, Sep. 2015.

[27] Q. Li, T. Zhang, G. Li, Z. Li, H. Xia, and C.-Y. Su, "Neural-dynamics optimization and repetitive learning control for robotic leg prostheses," *IEEE/ASME Trans. Mechatronics*, vol. 27, no. 2, pp. 811–822, Apr. 2022, doi: 10.1109/TMECH.2021.3071936.

[28] Q. Meng and Z. Hou, "Active disturbance rejection based repetitive learning control with applications in power inverters," *IEEE Trans. Control Syst. Technol.*, vol. 29, no. 5, pp. 2038–2048, Sep. 2021.

[29] Z. Chen, Z. Li, and C. L. P. Chen, "Adaptive neural control of uncertain MIMO nonlinear systems with state and input constraints," *IEEE Trans. Neural Netw. Learn. Syst.*, vol. 28, no. 6, pp. 1318–1330, Jun. 2017.

[30] T. Takenaka, T. Matsumoto, and T. Yoshiike, "Real time motion generation and control for biped robot-1st report: Walking gait pattern generation-," in *Proc. IEEE/RSJ Int. Conf. Intell. Robots Syst.*, 2009, pp. 1084–1091.

[31] M. Kasaei, N. Lau, and A. Pereira, "A robust biped locomotion based on linear-quadratic-Gaussian controller and divergent component of motion," in *Proc. IEEE/RSJ Int. Conf. Intell. Robots Syst.*, 2019, pp. 1429–1434.

[32] J. Englsberger, C. Ott, M. A. Roa, A. Albu-Schäffer, and G. Hirzinger, "Bipedal walking control based on capture point dynamics," in *Proc. IEEE/RSJ Int. Conf. Intell. Robots Syst.*, 2011, pp. 4420–4427.

[33] S. Caron, Q.-C. Pham, and Y. Nakamura, "ZMP support areas for multicontact mobility under frictional constraints," *IEEE Trans. Robot.*, vol. 33, no. 1, pp. 67–80, Feb. 2017.

[34] H. Yali and W. Xingsong, "Kinematics analysis of lower extremity exoskeleton," in *Proc. Chin. Control Decis. Conf.*, 2008, pp. 2837–2842.

[35] B. Brahmi, M. Saad, M. H. Rahman, and C. Ochoa-Luna, "Cartesian trajectory tracking of a 7-DOF exoskeleton robot based on human inverse kinematics," *IEEE Trans. Syst., Man, Cybern., Syst.*, vol. 49, no. 3, pp. 600–611, Mar. 2019.

[36] Z. Yao, J. Li, and H. Su, "A terrain-based gait self-adjusting planning for powered prostheses," in *Proc. IEEE 6th Int. Conf. Adv. Robot. Mechatronics (ICARM)*, Chongqing, China, 2021, pp. 1–6.

[37] Y. Liu, Z. Li, H. Su, and C.-Y. Su, "Whole-body control of an autonomous mobile manipulator using series elastic actuators," *IEEE/ASME Trans. Mechatronics*, vol. 26, no. 2, pp. 657–667, Apr. 2021.

[38] Y. Chen, Z. Wang, B. Shen, and Q.-L. Han, "Local stabilization for multiple input-delay systems subject to saturating actuators: The continuous-time case," *IEEE Trans. Autom. Control*, vol. 67, no. 6, pp. 3090–3097, Jun. 2022, doi: 10.1109/TAC.2021.3092556.

[39] W. Huo et al., "Impedance modulation control of a lower-limb exoskeleton to assist sit-to-stand movements," *IEEE Trans. Robot.*, vol. 38, no. 2, pp. 1230–1249, Apr. 2022.

[40] S. S. Ge, C. C. Hang, and T. Zhang, "A direct adaptive controller for dynamic systems with a class of nonlinear parameterizations," *Automatica*, vol. 35, no. 4, pp. 741–747, 1999.

[41] M. Sun, "Adaptive controller designs for nonlinear periodic systems," in *Proc. IEEE Int. Conf. Intell. Comput. Intell. Syst.*, Shanghai, China, 2009, pp. 798–802.

[42] C.-Y. Su, T.-P. Leung, and Y. Stepanenko, "Real-time implementation of regressor-based sliding mode control algorithm for robotic manipulators," *IEEE Trans. Ind. Electron.*, vol. 40, no. 1, pp. 71–79, Feb. 1993.
[43] L. Zhang, Z. Li, and C. Yang, "Adaptive neural network based variable stiffness control of uncertain robotic systems using disturbance observer," *IEEE Trans. Ind. Electron.*, vol. 64, no. 3, pp. 2236–2245, Mar. 2017.
[44] M. Sun and S. S. Ge, "Adaptive repetitive control for a class of nonlinearly parametrized systems," *IEEE Trans. Autom. Control*, vol. 51, no. 10, pp. 1684–1688, Oct. 2006.
[45] X. Li, Y. Lan, P. Jiang, H. Cao, and J. Zhou, "An efficient computation for energy optimization of robot trajectory," *IEEE Trans. Ind. Electron.*, vol. 69, no. 11, pp. 11436–11446, Nov. 2022, doi: 10.1109/TIE.2021.3118367.
[46] S. P. Madruga, A. H. B. M. Tavares, S. O. D. Luiz, T. P. do Nascimento, and A. M. N. Lima, "Aerodynamic effects compensation on multi-rotor UAVs based on a neural network control allocation approach," *IEEE/CAA J. Automatica Sinica*, vol. 9, no. 2, pp. 295–312, Feb. 2022.
[47] X. Lyu and Z. Lin, "PID control of planar nonlinear uncertain systems in the presence of actuator saturation," *IEEE/CAA J. Automatica Sinica*, vol. 9, no. 1, pp. 90–98, Jan. 2022.
[48] B. Li and B. Chen, "An adaptive rapidly-exploring random tree," *IEEE/CAA J. Automatica Sinica*, vol. 9, no. 2, pp. 283–294, Feb. 2022.
[49] B. Hu, Z. Cao, and M. Zhou, "An efficient RRT-based framework for planning short and smooth wheeled robot motion under kinodynamic constraints," *IEEE Trans. Ind. Electron.*, vol. 68, no. 4, pp. 3292–3302, Apr. 2021,

Pengbo Huang (Graduate Student Member, IEEE) received the B.S. degree in automation from the University of Science and Technology of China, Hefei, China, in 2020, where he is currently pursuing the M.S. degree in control science and engineering.

His current research interests include lower limb exoskeleton, adaptive control, and motion control design.

Zhijun Li (Fellow, IEEE) received the Ph.D. degree in mechatronics from Shanghai Jiao Tong University, Shanghai, China, in 2002.

He is currently a Chair Professor with the University of Science and Technology of China, Hefei, China, where he has been the Vice Dean of the School of Information Science and Technology since 2019. From 2003 to 2006, he was a Postdoctoral Fellow with the University of Electro-Communications, Tokyo, Japan, and the National University of Singapore, Singapore. He has published over 400 papers, where the prestigious contributions were wearable robotics and bio-mechatronics systems.

Dr. Li has received the Distinguished Lecturer (RAS), the Web of Science Highly Cited Researcher in 2019–2022, the 2018 National Ten-Thousand Talents Program in China, and the 2016 National Distinguished Young Scholar (NSFC).

MengChu Zhou (Fellow, IEEE) received the B.S. degree in control engineering from the Nanjing University of Science and Technology, Nanjing, China, in 1983, the M.S. degree in automatic control from the Beijing Institute of Technology, Beijing, China, in 1986, and the Ph.D. degree in computer and systems engineering from Rensselaer Polytechnic Institute, Troy, NY, USA, in 1990.

He joined New Jersey Institute of Technology, Newark, NJ, USA, in 1990, where he is currently a Distinguished Professor of Electrical and Computer Engineering. He has over 1000 publications, including 14 books, over 700 journal papers (over 600 in IEEE TRANSACTIONS), and 30 book-chapters. He holds 31 patents and several pending ones. His recently coauthored/edited books include *Sustainable Manufacturing Systems: An Energy Perspective* (IEEE Press/Wiley, Hoboken, NJ, USA, 2022) (with L. Li) and *Supervisory Control and Scheduling of Resource Allocation Systems: Reachability Graph Perspective* (IEEE Press/Wiley, Hoboken, NJ, USA, 2020) (with B. Huang). His research interests include Petri nets, intelligent automation, Internet of Things, big data, Web services, and intelligent transportation.

Dr. Zhou is a recipient of Humboldt Research Award for U.S. Senior Scientists from Alexander von Humboldt Foundation, the Franklin V. Taylor Memorial Award and the Norbert Wiener Award from IEEE Systems, Man and Cybernetics Society, and Excellence in Research Prize and Medal from New Jersey Institute of Technology. He is the Founding Editor of IEEE Press Book Series on Systems Science and Engineering and the Editor-in-Chief of IEEE/CAA JOURNAL OF AUTOMATICA SINICA. He is a Life Member of Chinese Association for Science and Technology-USA and served as its the President in 1999. He is a Fellow of International Federation of Automatic Control, American Association for the Advancement of Science, Chinese Association of Automation and National Academy of Inventors.

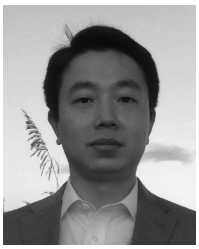

Zhen Kan (Senior Member, IEEE) received the Ph.D. degree in mechanical and aerospace engineering from the University of Florida, Gainesville, FL, USA, in 2011.

He was a Postdoctoral Research Fellow with the Air Force Research Laboratory, Eglin AFB, FL, USA, and the University of Florida Research and Engineering Education Facility, Shalimar, FL, USA, from 2012 to 2016 and was an Assistant Professor with the Department of Mechanical Engineering, University of Iowa, Iowa City, IA, USA, from 2016 to 2019. He is currently a Professor with the Department of Automation, University of Science and Technology of China, Hefei, China. His research interests include networked control systems, nonlinear control, formal methods, and robotics.

Prof. Kan currently serves on program committees of several internationally recognized scientific and engineering conferences and is an Associate Editor for IEEE TRANSACTIONS ON AUTOMATIC CONTROL.